Charge correlations using the balance function in Pb–Pb collisions at $\sqrt{s_{NN}} = 2.76$ TeV

Betty Abelev[bs], Jaroslav Adam[ak], Dagmar Adamova[bz], Andrew Marshall Adare[dw], Madan Aggarwal[cd], Gianluca Aglieri Rinella[ag], Michelangelo Agnello[cx,cj], Andras Gabor Agocs[dv], Andrea Agostinelli[aa], Zubayer Ahammed[dr], Nazeer Ahmad[q], Arshad Ahmad[q], Sang Un Ahn[an,bl], Sul-Ah Ahn[bl], Muhammad Ajaz[o], Alexander Akindinov[ax], Dmitry Aleksandrov[cp], Bruno Alessandro[cx], Andrea Alici[ct,l], Anton Alkin[c], Erick Jonathan Almaraz Avina[bh], Johan Alme[ai], Torsten Alt[am], Valerio Altini[ae], Sedat Altinpinar[r], Igor Altsybeev[ds], Cristian Andrei[bv], Anton Andronic[cm], Venelin Anguelov[ci], Jonas Anielski[bf], Christopher Daniel Anson[s], Tome Anticic[cn], Federico Antinori[cu], Pietro Antonioli[ct], Laurent Bernard Aphecetche[dc], Harald Appelshauser[bd], Nicolas Arbor[bo], Silvia Arcelli[aa], Andreas Arend[bd], Nestor Armesto[p], Roberta Arnaldi[cx], Tomas Robert Aronsson[dw], Ionut Cristian Arsene[cm], Mesut Arslandok[bd], Andzhey Asryan[ds], Andre Augustinus[ag], Ralf Peter Averbeck[cm], Terry Awes[ca], Juha Heikki Aysto[ap], Mohd Danish Azmi[q,cf], Matthias Jakob Bach[am], Angela Badala[da], Yong Wook Baek[bn,an], Raphaelle Marie Bailhache[bd], Renu Bala[cg,cx], Rinaldo Baldini Ferroli[l], Alberto Baldisseri[n], Fernando Baltasar Dos Santos Pedrosa[ag], Jaroslav Ban[ay], Rama Chandra Baral[az], Roberto Barbera[z], Francesco Barile[ae], Gergely Gabor Barnafoldi[dv], Lee Stuart Barnby[cr], Valerie Barret[bn], Jerzy Gustaw Bartke[df], Maurizio Basile[aa], Nicole Bastid[bn], Sumit Basu[dr], Bastian Bathen[bf], Guillaume Batigne[dc], Boris Batyunya[bj], Christoph Heinrich Baumann[bd], Ian Gardner Bearden[bx], Hans Beck[bd], Nirbhay Kumar Behera[ar], Iouri Belikov[bi], Francesca Bellini[aa], Rene Bellwied[dl], Ernesto Belmont-Moreno[bh], Gyula Bencedi[dv], Stefania Beole[v], Ionela Berceanu[bv], Alexandru Bercuci[bv], Yaroslav Berdnikov[cb], Daniel Berenyi[dv], Anais Annick Erica Bergognon[dc], Dario Berzano[v,cx], Latchezar Betev[ag], Anju Bhasin[cg], Ashok Kumar Bhati[cd], Jihyun Bhom[dp], Nicola Bianchi[bp], Livio Bianchi[v], Jaroslav Bielcik[ak], Jana Bielcikova[bz], Ante Bilandzic[bx], Sandro Bjelogrlic[aw], Francesco Blanco[dl], F. Blanco[j], Dmitry

[1]M.V.Lomonosov Moscow State University, D.V.Skobeltsyn Institute of Nuclear Physics, Moscow, Russia

[2]University of Belgrade, Faculty of Physics and "Vinča" Institute of Nuclear Sciences, Belgrade, Serbia

Blau[cp], Christoph Blume[bd], Marco Boccioli[ag], Stefan Boettger[bc], Alexey Bogdanov[bt], Hans Boggild[bx], Mikhail Bogolyubsky[au], Laszlo Boldizsar[dv], Marek Bombara[al], Julian Book[bd], Herve Borel[n], Alexander Borissov[du], Francesco Bossu[cf], Michiel Botje[by], Elena Botta[v], Ermes Braidot[br], Peter Braun-Munzinger[cm], Marco Bregant[dc], Timo Gunther Breitner[bc], Theo Alexander Broker[bd], Tyler Allen Browning[ck], Michal Broz[aj], Rene Brun[ag], Elena Bruna[v,cx], Giuseppe Eugenio Bruno[ae], Dmitry Budnikov[co], Henner Buesching[bd], Stefania Bufalino[v,cx], Predrag Buncic[ag], Oliver Busch[ci], Edith Zinhle Buthelezi[cf], Diego Caballero Orduna[dw], Davide Caffarri[ab,cu], Xu Cai[g], Helen Louise Caines[dw], Ernesto Calvo Villar[cs], Paolo Camerini[x], Veronica Canoa Roman[k], Giovanni Cara Romeo[ct], Francesco Carena[ag], Wisla Carena[ag], Nelson Carlin Filho[di], Federico Carminati[ag], Amaya Ofelia Casanova Diaz[bp], Javier Ernesto Castillo Castellanos[n], Juan Francisco Castillo Hernandez[cm], Ester Anna Rita Casula[w], Vasile Catanescu[bv], Costanza Cavicchioli[ag], Cesar Ceballos Sanchez[i], Jan Cepila[ak], Piergiorgio Cerello[cx], Beomsu Chang[ap,dy], Sylvain Chapeland[ag], Jean-Luc Fernand Charvet[n], Subhasis Chattopadhyay[dr], Sukalyan Chattopadhyay[cq], Isha Chawla[cd], Michael Gerard Cherney[cc], Cvetan Cheshkov[ag,dk], Brigitte Cheynis[dk], Vasco Miguel Chibante Barroso[ag], David Chinellato[dl], Peter Chochula[ag], Marek Chojnacki[bx], Subikash Choudhury[dr], Panagiotis Christakoglou[by], Christian Holm Christensen[bx], Peter Christiansen[af], Tatsuya Chujo[dp], Suh-Urk Chung[cl], Corrado Cicalo[cw], Luisa Cifarelli[aa,ag,l], Federico Cindolo[ct], Jean Willy Andre Cleymans[cf], Fabrizio Coccetti[l], Fabio Colamaria[ae], Domenico Colella[ae], Alberto Collu[w], Gustavo Conesa Balbastre[bo], Zaida Conesa del Valle[ag], Megan Elizabeth Connors[dw], Giacomo Contin[x], Jesus Guillermo Contreras[k], Thomas Michael Cormier[du], Yasser Corrales Morales[v], Pietro Cortese[ad], Ismael Cortes Maldonado[b], Mauro Rogerio Cosentino[br], Filippo Costa[ag], Manuel Enrique Cotallo[j], Elisabetta Crescio[k], Philippe Crochet[bn], Emilia Cruz Alaniz[bh], Rigoberto Cruz Albino[k], Eleazar Cuautle[bg], Leticia Cunqueiro[bp], Andrea Dainese[ab,cu], Hans Hjersing Dalsgaard[bx], Andrea Danu[bb], Supriya Das[d], Debasish Das[cq], Kushal Das[cq], Indranil Das[at], Sadhana Dash[ar], Ajay Kumar Dash[dj], Sudipan De[dr], Gabriel de Barros[di], Annalisa De Caro[ac,l], Giacinto de Cataldo[cz], Jan de Cuveland[am], Alessandro De Falco[w], Daniele De Gruttola[ac,l], Hugues Delagrange[dc], Andrzej Deloff[bu], Nora De Marco[cx], Ervin Denes[dv], Salvatore De Pasquale[ac], Airton Deppman[di], Ginevra D'Erasmo[ae], Raoul Stefan de Rooij[aw], Miguel Angel Diaz Corchero[j], Domenico Di Bari[ae], Thomas Dietel[bf], Carmelo Di Giglio[ae], Sergio Di

Liberto[cv], Antonio Di Mauro[ag], Pasquale Di Nezza[bp], Roberto Divia[ag], Oeystein Djuvsland[r], Alexandru Florin Dobrin[du,af], Tadeusz Antoni Dobrowolski[bu], Benjamin Donigus[cm], Olja Dordic[u], Olga Driga[dc], Anand Kumar Dubey[dr], Andrea Dubla[aw], Laurent Ducroux[dk], Pascal Dupieux[bn], A.K. Dutta Majumdar[cq], Domenico Elia[cz], David Philip Emschermann[bf], Heiko Engel[bc], Barbara Erazmus[ag,dc], Hege Austrheim Erdal[ai], Bruno Espagnon[at], Magali Danielle Estienne[dc], Shinichi Esumi[dp], David Evans[cr], Gyulnara Eyyubova[u], Daniela Fabris[ab,cu], Julien Faivre[bo], Davide Falchieri[aa], Alessandra Fantoni[bp], Markus Fasel[cm,ci], Roger Worsley Fearick[cf], Dominik Fehlker[r], Linus Feldkamp[bf], Daniel Felea[bb], Alessandro Feliciello[cx], Bo Fenton-Olsen[br], Grigory Feofilov[ds], Arturo Fernandez Tellez[b], Alessandro Ferretti[v], Andrea Festanti[ab], Jan Figiel[df], Marcel Figueredo[di], Sergey Filchagin[co], Dmitry Finogeev[av], Fiorella Fionda[ae], Enrichetta Maria Fiore[ae], Emmanuel Floratos[ce], Michele Floris[ag], Siegfried Valentin Foertsch[cf], Panagiota Foka[cm], Sergey Fokin[cp], Enrico Fragiacomo[cy], Andrea Francescon[ag,ab], Ulrich Michael Frankenfeld[cm], Ulrich Fuchs[ag], Christophe Furget[bo], Mario Fusco Girard[ac], Jens Joergen Gaardhoje[bx], Martino Gagliardi[v], Alberto Gago[cs], Mauro Gallio[v], Dhevan Raja Gangadharan[s], Paraskevi Ganoti[ca], Jose Garabatos[cm], Edmundo Garcia-Solis[m], Corrado Gargiulo[ag], Irakli Garishvili[bs], Jochen Gerhard[am], Marie Germain[dc], Claudio Geuna[n], Andrei George Gheata[ag], Mihaela Gheata[bb,ag], Bruno Ghidini[ae], Premomoy Ghosh[dr], Paola Gianotti[bp], Martin Robert Girard[dt], Paolo Giubellino[ag], Ewa Gladysz-Dziadus[df], Peter Glassel[ci], Ramon Gomez[dh,k], Elena Gonzalez Ferreiro[p], Laura Helena Gonzalez-Trueba[bh], Pedro Gonzalez-Zamora[j], Sergey Gorbunov[am], Ankita Goswami[ch], Sven Gotovac[de], Lukasz Kamil Graczykowski[dt], Robert Grajcarek[ci], Alessandro Grelli[aw], Costin Grigoras[ag], Alina Gabriela Grigoras[ag], Vladislav Grigoriev[bt], Ara Grigoryan[a], Smbat Grigoryan[bj], Boris Grinyov[c], Nevio Grion[cy], Philippe Gros[af], Jan Fiete Grosse-Oetringhaus[ag], Jean-Yves Grossiord[dk], Raffaele Grosso[ag], Fedor Guber[av], Rachid Guernane[bo], Barbara Guerzoni[aa], Maxime Rene Joseph Guilbaud[dk], Kristjan Herlache Gulbrandsen[bx], Hrant Gulkanyan[a], Taku Gunji[do], Anik Gupta[cg], Ramni Gupta[cg], Rudiger Haake[bf], Oystein Senneset Haaland[r], Cynthia Marie Hadjidakis[at], Maria Haiduc[bb], Hideki Hamagaki[do], Gergoe Hamar[dv], Byounghee Han[t], Luke David Hanratty[cr], Alexander Hansen[bx], Zuzana Harmanova[al], John William Harris[dw], Matthias Hartig[bd], Austin Harton[m], Despoina Hatzifotiadou[ct], Shinichi Hayashi[do], Arsen Hayrapetyan[ag,a], Stefan Thomas Heckel[bd], Markus Ansgar Heide[bf], Haavard

Helstrup[ai], Andrei Ionut Herghelegiu[bv], Gerardo Antonio Herrera Corral[k], Norbert Herrmann[ci], Benjamin Andreas Hess[dq], Kristin Fanebust Hetland[ai], Bernard Hicks[dw], Boris Hippolyte[bi], Yasuto Hori[do], Peter Zahariev Hristov[ag], Ivana Hrivnacova[at], Meidana Huang[r], Thomas Humanic[s], Dae Sung Hwang[t], Raphaelle Ichou[bn], Radiy Ilkaev[co], Iryna Ilkiv[bu], Motoi Inaba[dp], Elisa Incani[w], Pier Giorgio Innocenti[ag], Gian Michele Innocenti[v], Mikhail Ippolitov[cp], Muhammad Irfan[q], Cristian George Ivan[cm], Vladimir Ivanov[cb], Andrey Ivanov[ds], Marian Ivanov[cm], Oleksii Ivanytskyi[c], Adam Wlodzimierz Jacholkowski[z], Peter Jacobs[br], Haeng Jin Jang[bl], Malgorzata Anna Janik[dt], Rudolf Janik[aj], Sandun Jayarathna[dl], Satyajit Jena[ar], Deeptanshu Manu Jha[du], Raul Tonatiuh Jimenez Bustamante[bg], Peter Graham Jones[cr], Hyung Taik Jung[an], Anton Jusko[cr], Alexei Kaidalov[ax], Sebastian Kalcher[am], Peter Kalinak[ay], Tuomo Esa Aukusti Kalliokoski[ap], Alexander Philipp Kalweit[be,ag], Ju Hwan Kang[dy], Vladimir Kaplin[bt], Ayben Karasu Uysal[ag,dx,bm], Oleg Karavichev[av], Tatiana Karavicheva[av], Evgeny Karpechev[av], Andrey Kazantsev[cp], Udo Wolfgang Kebschull[bc], Ralf Keidel[dz], Palash Khan[cq], Shuaib Ahmad Khan[dr], Mohisin Mohammed Khan[q], Kamal Hussain Khan[o], Alexei Khanzadeev[cb], Yury Kharlov[au], Bjarte Kileng[ai], Taesoo Kim[dy], Se Yong Kim[t], Minwoo Kim[dy], Beomkyu Kim[dy], Mimae Kim[an], Jin Sook Kim[an], Jonghyun Kim[t], Dong Jo Kim[ap], Do Won Kim[an,bl], Stefan Kirsch[am], Ivan Kisel[am], Sergey Kiselev[ax], Adam Ryszard Kisiel[dt], Jennifer Lynn Klay[f], Jochen Klein[ci], Christian Klein-Bosing[bf], Michael Kliemant[bd], Alexander Kluge[ag], Michael Linus Knichel[cm], Anders Garritt Knospe[dg], Markus Kohler[cm], Thorsten Kollegger[am], Anatoly Kolojvari[ds], Mikhail Kompaniets[ds], Valery Kondratiev[ds], Natalia Kondratyeva[bt], Artem Konevskih[av], Vladimir Kovalenko[ds], Marek Kowalski[df], Serge Kox[bo], Greeshma Koyithatta Meethaleveedu[ar], Jiri Kral[ap], Ivan Kralik[ay], Frederick Kramer[bd], Adela Kravcakova[al], Tobias Krawutschke[ci,ah], Michal Krelina[ak], Matthias Kretz[am], Marian Krivda[cr,ay], Filip Krizek[ap], Miroslav Krus[ak], Evgeny Kryshen[cb], Mikolaj Krzewicki[cm], Yury Kucheriaev[cp], Thanushan Kugathasan[ag], Christian Claude Kuhn[bi], Paul Kuijer[by], Igor Kulakov[bd], Jitendra Kumar[ar], Podist Kurashvili[bu], A.B. Kurepin[av], A. Kurepin[av], Alexey Kuryakin[co], Vasily Kushpil[bz], Svetlana Kushpil[bz], Henning Kvaerno[u], Min Jung Kweon[ci], Youngil Kwon[dy], Pedro Ladron de Guevara[bg], Igor Lakomov[at], Rune Langoy[r], Sarah Louise La Pointe[aw], Camilo Ernesto Lara[bc], Antoine Xavier Lardeux[dc], Paola La Rocca[z], Ramona Lea[x], Mateusz Lechman[ag], Ki Sang Lee[an], Sung Chul Lee[an], Graham Richard Lee[cr], Iosif Legrand[ag], Joerg

Walter Lehnert[bd], Matthieu Laurent Lenhardt[cm], Vito Lenti[cz], Hermes Leon[bh], Ildefonso Leon Monzon[dh], Hermes Leon Vargas[bd], Peter Levai[dv], Shuang Li[g], Jorgen Lien[r], Roman Lietava[cr], Svein Lindal[u], Volker Lindenstruth[am], Christian Lippmann[cm,ag], Michael Annan Lisa[s], Hans Martin Ljunggren[af], Davide Francesco Lodato[aw], Per-Ivar Loenne[r], Vera Loggins[du], Vitaly Loginov[bt], Daniel Lohner[ci], Constantinos Loizides[br], Kai Krister Loo[ap], Xavier Bernard Lopez[bn], Ernesto Lopez Torres[i], Gunnar Lovhoiden[u], Xianguo Lu[ci], Philipp Luettig[bd], Marcello Lunardon[ab], Jiebin Luo[g], Grazia Luparello[aw], Cinzia Luzzi[ag], Rongrong Ma[dw], Ke Ma[g], Dilan Minthaka Madagodahettige-Don[dl], Alla Maevskaya[av], Magnus Mager[be,ag], Durga Prasad Mahapatra[az], Antonin Maire[ci], Mikhail Malaev[cb], Ivonne Alicia Maldonado Cervantes[bg], Ludmila Malinina[bj,1], Dmitry Mal'Kevich[ax], Peter Malzacher[cm], Alexander Mamonov[co], Loic Henri Antoine Manceau[cx], Lalit Kumar Mangotra[cg], Vladislav Manko[cp], Franck Manso[bn], Vito Manzari[cz], Yaxian Mao[g], Massimiliano Marchisone[bn,v], Jiri Mares[ba], Giacomo Vito Margagliotti[x,cy], Anselmo Margotti[ct], Ana Maria Marin[cm], Christina Markert[dg], Marco Marquard[bd], Irakli Martashvili[dn], Nicole Alice Martin[cm], Paolo Martinengo[ag], Mario Ivan Martinez[b], Arnulfo Martinez Davalos[bh], Gines Martinez Garcia[dc], Yevgen Martynov[c], Alexis Jean-Michel Mas[dc], Silvia Masciocchi[cm], Massimo Masera[v], Alberto Masoni[cw], Laure Marie Massacrier[dc], Annalisa Mastroserio[ae], Adam Tomasz Matyja[df], Christoph Mayer[df], Joel Mazer[dn], Alessandra Maria Mazzoni[cv], Franco Meddi[y], Arturo Alejandro Menchaca-Rocha[bh], Jorge Mercado Perez[ci], Michal Meres[aj], Yasuo Miake[dp], Leonardo Milano[v], Jovan Milosevic[u,2], Andre Mischke[aw], Aditya Nath Mishra[ch,as], Dariusz Miskowiec[cm], Ciprian Mihai Mitu[bb], Sanshiro Mizuno[dp], Jocelyn Mlynarz[du], Bedangadas Mohanty[dr,bw], Levente Molnar[dv,ag,bi], Luis Manuel Montano Zetina[k], Marco Monteno[cx], Esther Montes[j], Taebong Moon[dy], Maurizio Morando[ab], Denise Aparecida Moreira De Godoy[di], Sandra Moretto[ab], Astrid Morreale[ap], Andreas Morsch[ag], Valeria Muccifora[bp], Eugen Mudnic[de], Sanjib Muhuri[dr], Maitreyee Mukherjee[dr], Hans Muller[ag], Marcelo Munhoz[di], Sean Murray[cf], Luciano Musa[ag], Jan Musinsky[ay], Alfredo Musso[cx], Basanta Kumar Nandi[ar], Rosario Nania[ct], Eugenio Nappi[cz], Christine Nattrass[dn], Tapan Kumar Nayak[dr], Sergey Nazarenko[co], Alexander Nedosekin[ax], Maria Nicassio[ae,cm], Mihai Niculescu[bb,ag], Borge Svane Nielsen[bx], Takafumi Niida[dp], Sergey Nikolaev[cp], Vedran Nikolic[cn], Sergey Nikulin[cp], Vladimir Nikulin[cb], Bjorn Steven Nilsen[cc], Mads Stormo Nilsson[u], Francesco Noferini[ct,l], Petr Nomokonov[bj], Gerardus Nooren[aw], Norbert Novitzky[ap],

Alexandre Nyanin[cp], Anitha Nyatha[ar], Casper Nygaard[bx], Joakim Ingemar Nystrand[r], Alexander Ochirov[ds], Helmut Oskar Oeschler[be,ag], Saehanseul Oh[dw], Sun Kun Oh[an], Janusz Oleniacz[dt], Antonio Carlos Oliveira Da Silva[di], Chiara Oppedisano[cx], Antonio Ortiz Velasquez[af,bg], Anders Nils Erik Oskarsson[af], Piotr Krystian Ostrowski[dt], Jacek Tomasz Otwinowski[cm], Ken Oyama[ci], Kyoichiro Ozawa[do], Yvonne Chiara Pachmayer[ci], Milos Pachr[ak], Fatima Padilla[v], Paola Pagano[ac], Guy Paic[bg], Florian Painke[am], Carlos Pajares[p], Susanta Kumar Pal[dr], Arvinder Singh Palaha[cr], Armando Palmeri[da], Vardanush Papikyan[a], Giuseppe Pappalardo[da], Woo Jin Park[cm], Annika Passfeld[bf], Blahoslav Pastircak[ay], Dmitri Ivanovich Patalakha[au], Vincenzo Paticchio[cz], Biswarup Paul[cq], Alexei Pavlinov[du], Tomasz Jan Pawlak[dt], Thomas Peitzmann[aw], Hugo Denis Antonio Pereira Da Costa[n], Elienos Pereira De Oliveira Filho[di], Dmitri Peresunko[cp], Carlos Eugenio Perez Lara[by], Diego Perini[ag], Davide Perrino[ae], Wiktor Stanislaw Peryt[dt], Alessandro Pesci[ct], Vladimir Peskov[ag,bg], Yury Pestov[e], Vojtech Petracek[ak], Michal Petran[ak], Mariana Petris[bv], Plamen Rumenov Petrov[cr], Mihai Petrovici[bv], Catia Petta[z], Stefano Piano[cy], Miroslav Pikna[aj], Philippe Pillot[dc], Ombretta Pinazza[ag], Lawrence Pinsky[dl], Nora Pitz[bd], Danthasinghe Piyarathna[dl], Mirko Planinic[cn], Mateusz Andrzej Ploskon[br], Jan Marian Pluta[dt], Timur Pocheptsov[bj], Sona Pochybova[dv], Pedro Luis Manuel Podesta Lerma[dh], Martin Poghosyan[ag], Karel Polak[ba], Boris Polichtchouk[au], Amalia Pop[bv], Sarah Porteboeuf-Houssais[bn], Vladimir Pospisil[ak], Baba Potukuchi[cg], Sidharth Kumar Prasad[du], Roberto Preghenella[ct,l], Francesco Prino[cx], Claude Andre Pruneau[du], Igor Pshenichnov[av], Giovanna Puddu[w], Valery Punin[co], Marian Putis[al], Jorn Henning Putschke[du], Emanuele Quercigh[ag], Henrik Qvigstad[u], Alexandre Rachevski[cy], Alphonse Rademakers[ag], Tomi Samuli Raiha[ap], Jan Rak[ap], Andry Malala Rakotozafindrabe[n], Luciano Ramello[ad], Abdiel Ramirez Reyes[k], Rashmi Raniwala[ch], Sudhir Raniwala[ch], Sami Sakari Rasanen[ap], Bogdan Theodor Rascanu[bd], Deepika Rathee[cd], Kenneth Francis Read[dn], Jean-Sebastien Real[bo], Krzysztof Redlich[bu,1,1,1,1], Rosi Jan Reed[dw], Attiq Ur Rehman[r], Patrick Reichelt[bd], Martijn Reicher[aw], Rainer Arno Ernst Renfordt[bd], Anna Rita Reolon[bp], Andrey Reshetin[av], Felix Vincenz Rettig[am], Jean-Pierre Revol[ag], Klaus Johannes Reygers[ci], Lodovico Riccati[cx], Renato Angelo Ricci[bq], Tuva Richert[af], Matthias Rudolph Richter[u], Petra Riedler[ag], Werner Riegler[ag], Francesco Riggi[z,da], Mario Rodriguez Cahuantzi[b], Alis Rodriguez Manso[by], Ketil Roed[r,u], David Rohr[am], Dieter Rohrich[r], Rosa Romita[cm,db], Federico Ronchetti[bp], Philippe

Rosnet[bn], Stefan Rossegger[ag], Andrea Rossi[ag,ab], Pradip Kumar Roy[cq], Christelle Sophie Roy[bi], Antonio Juan Rubio Montero[j], Rinaldo Rui[x], Riccardo Russo[v], Evgeny Ryabinkin[cp], Andrzej Rybicki[df], Sergey Sadovsky[au], Karel Safarik[ag], Raghunath Sahoo[as], Pradip Kumar Sahu[az], Jogender Saini[dr], Hiroaki Sakaguchi[aq], Shingo Sakai[br], Dosatsu Sakata[dp], Carlos Albert Salgado[p], Jai Salzwedel[s], Sanjeev Singh Sambyal[cg], Vladimir Samsonov[cb], Xitzel Sanchez Castro[bi], Ladislav Sandor[ay], Andres Sandoval[bh], Masato Sano[dp], Gianluca Santagati[z], Romualdo Santoro[ag,l], Juho Jaako Sarkamo[ap], Eugenio Scapparone[ct], Fernando Scarlassara[ab], Rolf Paul Scharenberg[ck], Claudiu Cornel Schiaua[bv], Rainer Martin Schicker[ci], Hans Rudolf Schmidt[dq], Christian Joachim Schmidt[cm], Simone Schuchmann[bd], Jurgen Schukraft[ag], Tim Schuster[dw], Yves Roland Schutz[ag,dc], Kilian Eberhard Schwarz[cm], Kai Oliver Schweda[cm], Gilda Scioli[aa], Enrico Scomparin[cx], Rebecca Scott[dn], Patrick Aaron Scott[cr], Gianfranco Segato[ab], Ilya Selyuzhenkov[cm], Serhiy Senyukov[bi], Jeewon Seo[cl], Sergio Serci[w], Eulogio Serradilla[j,bh], Adrian Sevcenco[bb], Alexandre Shabetai[dc], Galina Shabratova[bj], Ruben Shahoyan[ag], Natasha Sharma[cd,dn], Satish Sharma[cg], Rohini Sharma[cg], Kenta Shigaki[aq], Katherin Shtejer[i], Yury Sibiriak[cp], Eva Sicking[bf], Sabyasachi Siddhanta[cw], Teodor Siemiarczuk[bu], David Olle Rickard Silvermyr[ca], Catherine Silvestre[bo], Goran Simatovic[bg,cn], Giuseppe Simonetti[ag], Rama Narayana Singaraju[dr], Ranbir Singh[cg], Subhash Singha[dr,bw], Vikas Singhal[dr], Tinku Sinha[cq], Bikash Sinha[dr], Branislav Sitar[aj], Mario Sitta[ad], Bernhard Skaali[u], Kyrre Skjerdal[r], Radek Smakal[ak], Nikolai Smirnov[dw], Raimond Snellings[aw], Carsten Sogaard[bx,af], Ron Ariel Soltz[bs], Hyungsuk Son[t], Jihye Song[cl], Myunggeun Song[dy], Csaba Soos[ag], Francesca Soramel[ab], Iwona Sputowska[df], Martha Spyropoulou-Stassinaki[ce], Brijesh Kumar Srivastava[ck], Johanna Stachel[ci], Ionel Stan[bb], Grzegorz Stefanek[bu], Matthew Steinpreis[s], Evert Anders Stenlund[af], Gideon Francois Steyn[cf], Johannes Hendrik Stiller[ci], Diego Stocco[dc], Mikhail Stolpovskiy[au], Peter Strmen[aj], Alexandre Alarcon do Passo Suaide[di], Martin Alfonso Subieta Vasquez[v], Toru Sugitate[aq], Christophe Pierre Suire[at], Rishat Sultanov[ax], Michal Sumbera[bz], Tatjana Susa[cn], Timothy Symons[br], Alejandro Szanto de Toledo[di], Imrich Szarka[aj], Adam Szczepankiewicz[df,ag], Maciej Szymanski[dt], Jun Takahashi[dj], Marco-Antonio Tangaro[ae], Daniel Jesus Tapia Takaki[at], Attilio Tarantola Peloni[bd], Alfonso Tarazona Martinez[ag], Arturo Tauro[ag], Guillermo Tejeda Munoz[b], Adriana Telesca[ag], Astkhik Ter-Minasyan[bt,cp], Cristina Terrevoli[ae], Jochen Mathias Thader[cm], Deepa Thomas[aw], Raphael Noel Tieulent[dk],

Anthony Timmins[dl], David Tlusty[ak], Alberica Toia[am,ab,cu], Hisayuki Torii[do], Luca Toscano[cx], Victor Trubnikov[c], David Christopher Truesdale[s], Wladyslaw Henryk Trzaska[ap], Tomoya Tsuji[do], Alexandr Tumkin[co], Rosario Turrisi[cu], Trine Spedstad Tveter[u], Jason Glyndwr Ulery[bd], Kjetil Ullaland[r], Jochen Ulrich[bk,bc], Antonio Uras[dk], Jozef Urban[al], Guido Marie Urciuoli[cv], Gianluca Usai[w], Michal Vajzer[ak,bz], Martin Vala[bj,ay], Lizardo Valencia Palomo[at], Sara Vallero[ci], Pierre Vande Vyvre[ag], Marco van Leeuwen[aw], Luigi Vannucci[bq], Aurora Diozcora Vargas[b], Raghava Varma[ar], Maria Vasileiou[ce], Andrey Vasiliev[cp], Vladimir Vechernin[ds], Misha Veldhoen[aw], Massimo Venaruzzo[x], Ermanno Vercellin[v], Sergio Vergara[b], Renaud Vernet[h], Marta Verweij[aw], Linda Vickovic[de], Giuseppe Viesti[ab], Jussi Viinikainen[ap], Zabulon Vilakazi[cf], Orlando Villalobos Baillie[cr], Yury Vinogradov[co], Alexander Vinogradov[cp], Leonid Vinogradov[ds], Tiziano Virgili[ac], Yogendra Viyogi[dr], Alexander Vodopianov[bj], Kirill Voloshin[ax], Sergey Voloshin[du], Giacomo Volpe[ag], Barthelemy von Haller[ag], Ivan Vorobyev[ds], Danilo Vranic[cm], Janka Vrlakova[al], Bogdan Vulpescu[bn], Alexey Vyushin[co], Vladimir Wagner[ak], Boris Wagner[r], Renzhuo Wan[g], Dong Wang[g], Yifei Wang[ci], Mengliang Wang[g], Yaping Wang[g], Kengo Watanabe[dp], Michael Weber[dl], Johannes Wessels[ag,bf], Uwe Westerhoff[bf], Jens Wiechula[dq], Jon Wikne[u], Martin Rudolf Wilde[bf], Grzegorz Andrzej Wilk[bu], Alexander Wilk[bf], Crispin Williams[ct], Bernd Stefan Windelband[ci], Leonidas Xaplanteris Karampatsos[dg], Chris G Yaldo[du], Yorito Yamaguchi[do], Shiming Yang[r], Hongyan Yang[n,aw], Stanislav Yasnopolsky[cp], JunGyu Yi[cl], Zhongbao Yin[g], In-Kwon Yoo[cl], Jongik Yoon[dy], Weilin Yu[bd], Xianbao Yuan[g], Igor Yushmanov[cp], Valentina Zaccolo[bx], Cenek Zach[ak], Chiara Zampolli[ct], Sergey Zaporozhets[bj], Andrey Zarochentsev[ds], Petr Zavada[ba], Nikolai Zaviyalov[co], Hanna Paulina Zbroszczyk[dt], Pierre Zelnicek[bc], Sorin Ion Zgura[bb], Mikhail Zhalov[cb], Xiaoming Zhang[br,bn,g], Haitao Zhang[g], Fengchu Zhou[g], You Zhou[aw], Daicui Zhou[g], Jianlin Zhu[g], Jianhui Zhu[g], Xiangrong Zhu[g], Hongsheng Zhu[g], Antonino Zichichi[aa,l], Alice Zimmermann[ci], Gennady Zinovjev[c], Yannick Denis Zoccarato[dk], Mykhaylo Zynovyev[c], Maksym Zyzak[bd]

[a] *A. I. Alikhanyan National Science Laboratory (Yerevan Physics Institute) Foundation, Yerevan, Armenia*

[b] *Benemérita Universidad Autónoma de Puebla, Puebla, Mexico*

[c] *Bogolyubov Institute for Theoretical Physics, Kiev, Ukraine*

[d] *Bose Institute, Department of Physics and Centre for Astroparticle Physics and Space Science (CAPSS), Kolkata, India*

[e]Budker Institute for Nuclear Physics, Novosibirsk, Russia
[f]California Polytechnic State University, San Luis Obispo, California, United States
[g]Central China Normal University, Wuhan, China
[h]Centre de Calcul de l'IN2P3, Villeurbanne, France
[i]Centro de Aplicaciones Tecnológicas y Desarrollo Nuclear (CEADEN), Havana, Cuba
[j]Centro de Investigaciones Energéticas Medioambientales y Tecnológicas (CIEMAT), Madrid, Spain
[k]Centro de Investigación y de Estudios Avanzados (CINVESTAV), Mexico City and Mérida, Mexico
[l]Centro Fermi - Museo Storico della Fisica e Centro Studi e Ricerche "Enrico Fermi", Rome, Italy
[m]Chicago State University, Chicago, United States
[n]Commissariat à l'Energie Atomique, IRFU, Saclay, France
[o]COMSATS Institute of Information Technology (CIIT), Islamabad, Pakistan
[p]Departamento de Física de Partículas and IGFAE, Universidad de Santiago de Compostela, Santiago de Compostela, Spain
[q]Department of Physics Aligarh Muslim University, Aligarh, India
[r]Department of Physics and Technology, University of Bergen, Bergen, Norway
[s]Department of Physics, Ohio State University, Columbus, Ohio, United States
[t]Department of Physics, Sejong University, Seoul, South Korea
[u]Department of Physics, University of Oslo, Oslo, Norway
[v]Dipartimento di Fisica dell'Università and Sezione INFN, Turin, Italy
[w]Dipartimento di Fisica dell'Università and Sezione INFN, Cagliari, Italy
[x]Dipartimento di Fisica dell'Università and Sezione INFN, Trieste, Italy
[y]Dipartimento di Fisica dell'Università 'La Sapienza' and Sezione INFN, Rome, Italy
[z]Dipartimento di Fisica e Astronomia dell'Università and Sezione INFN, Catania, Italy
[aa]Dipartimento di Fisica e Astronomia dell'Università and Sezione INFN, Bologna, Italy
[ab]Dipartimento di Fisica e Astronomia dell'Università and Sezione INFN, Padova, Italy
[ac]Dipartimento di Fisica 'E.R. Caianiello' dell'Università and Gruppo Collegato INFN, Salerno, Italy
[ad]Dipartimento di Scienze e Innovazione Tecnologica dell'Università del Piemonte Orientale and Gruppo Collegato INFN, Alessandria, Italy
[ae]Dipartimento Interateneo di Fisica 'M. Merlin' and Sezione INFN, Bari, Italy
[af]Division of Experimental High Energy Physics, University of Lund, Lund, Sweden
[ag]European Organization for Nuclear Research (CERN), Geneva, Switzerland
[ah]Fachhochschule Köln, Köln, Germany
[ai]Faculty of Engineering, Bergen University College, Bergen, Norway
[aj]Faculty of Mathematics, Physics and Informatics, Comenius University, Bratislava, Slovakia
[ak]Faculty of Nuclear Sciences and Physical Engineering, Czech Technical University in Prague, Prague, Czech Republic
[al]Faculty of Science, P.J. Šafárik University, Košice, Slovakia
[am]Frankfurt Institute for Advanced Studies, Johann Wolfgang Goethe-Universität Frankfurt, Frankfurt, Germany
[an]Gangneung-Wonju National University, Gangneung, South Korea

[ao] Gauhati University, Department of Physics, Guwahati, India
[ap] Helsinki Institute of Physics (HIP) and University of Jyväskylä, Jyväskylä, Finland
[aq] Hiroshima University, Hiroshima, Japan
[ar] Indian Institute of Technology Bombay (IIT), Mumbai, India
[as] Indian Institute of Technology Indore, Indore, India (IITI)
[at] Institut de Physique Nucléaire d'Orsay (IPNO), Université Paris-Sud, CNRS-IN2P3, Orsay, France
[au] Institute for High Energy Physics, Protvino, Russia
[av] Institute for Nuclear Research, Academy of Sciences, Moscow, Russia
[aw] Nikhef, National Institute for Subatomic Physics and Institute for Subatomic Physics of Utrecht University, Utrecht, Netherlands
[ax] Institute for Theoretical and Experimental Physics, Moscow, Russia
[ay] Institute of Experimental Physics, Slovak Academy of Sciences, Košice, Slovakia
[az] Institute of Physics, Bhubaneswar, India
[ba] Institute of Physics, Academy of Sciences of the Czech Republic, Prague, Czech Republic
[bb] Institute of Space Sciences (ISS), Bucharest, Romania
[bc] Institut für Informatik, Johann Wolfgang Goethe-Universität Frankfurt, Frankfurt, Germany
[bd] Institut für Kernphysik, Johann Wolfgang Goethe-Universität Frankfurt, Frankfurt, Germany
[be] Institut für Kernphysik, Technische Universität Darmstadt, Darmstadt, Germany
[bf] Institut für Kernphysik, Westfälische Wilhelms-Universität Münster, Münster, Germany
[bg] Instituto de Ciencias Nucleares, Universidad Nacional Autónoma de México, Mexico City, Mexico
[bh] Instituto de Física, Universidad Nacional Autónoma de México, Mexico City, Mexico
[bi] Institut Pluridisciplinaire Hubert Curien (IPHC), Université de Strasbourg, CNRS-IN2P3, Strasbourg, France
[bj] Joint Institute for Nuclear Research (JINR), Dubna, Russia
[bk] Kirchhoff-Institut für Physik, Ruprecht-Karls-Universität Heidelberg, Heidelberg, Germany
[bl] Korea Institute of Science and Technology Information, Daejeon, South Korea
[bm] KTO Karatay University, Konya, Turkey
[bn] Laboratoire de Physique Corpusculaire (LPC), Clermont Université, Université Blaise Pascal, CNRS–IN2P3, Clermont-Ferrand, France
[bo] Laboratoire de Physique Subatomique et de Cosmologie (LPSC), Université Joseph Fourier, CNRS-IN2P3, Institut Polytechnique de Grenoble, Grenoble, France
[bp] Laboratori Nazionali di Frascati, INFN, Frascati, Italy
[bq] Laboratori Nazionali di Legnaro, INFN, Legnaro, Italy
[br] Lawrence Berkeley National Laboratory, Berkeley, California, United States
[bs] Lawrence Livermore National Laboratory, Livermore, California, United States
[bt] Moscow Engineering Physics Institute, Moscow, Russia
[bu] National Centre for Nuclear Studies, Warsaw, Poland
[bv] National Institute for Physics and Nuclear Engineering, Bucharest, Romania

[bw]National Institute of Science Education and Research, Bhubaneswar, India
[bx]Niels Bohr Institute, University of Copenhagen, Copenhagen, Denmark
[by]Nikhef, National Institute for Subatomic Physics, Amsterdam, Netherlands
[bz]Nuclear Physics Institute, Academy of Sciences of the Czech Republic, Řež u Prahy, Czech Republic
[ca]Oak Ridge National Laboratory, Oak Ridge, Tennessee, United States
[cb]Petersburg Nuclear Physics Institute, Gatchina, Russia
[cc]Physics Department, Creighton University, Omaha, Nebraska, United States
[cd]Physics Department, Panjab University, Chandigarh, India
[ce]Physics Department, University of Athens, Athens, Greece
[cf]Physics Department, University of Cape Town and iThemba LABS, National Research Foundation, Somerset West, South Africa
[cg]Physics Department, University of Jammu, Jammu, India
[ch]Physics Department, University of Rajasthan, Jaipur, India
[ci]Physikalisches Institut, Ruprecht-Karls-Universität Heidelberg, Heidelberg, Germany
[cj]Politecnico di Torino, Turin, Italy
[ck]Purdue University, West Lafayette, Indiana, United States
[cl]Pusan National University, Pusan, South Korea
[cm]Research Division and ExtreMe Matter Institute EMMI, GSI Helmholtzzentrum für Schwerionenforschung, Darmstadt, Germany
[cn]Rudjer Bošković Institute, Zagreb, Croatia
[co]Russian Federal Nuclear Center (VNIIEF), Sarov, Russia
[cp]Russian Research Centre Kurchatov Institute, Moscow, Russia
[cq]Saha Institute of Nuclear Physics, Kolkata, India
[cr]School of Physics and Astronomy, University of Birmingham, Birmingham, United Kingdom
[cs]Sección Física, Departamento de Ciencias, Pontificia Universidad Católica del Perú, Lima, Peru
[ct]Sezione INFN, Bologna, Italy
[cu]Sezione INFN, Padova, Italy
[cv]Sezione INFN, Rome, Italy
[cw]Sezione INFN, Cagliari, Italy
[cx]Sezione INFN, Turin, Italy
[cy]Sezione INFN, Trieste, Italy
[cz]Sezione INFN, Bari, Italy
[da]Sezione INFN, Catania, Italy
[db]Nuclear Physics Group, STFC Daresbury Laboratory, Daresbury, United Kingdom
[dc]SUBATECH, Ecole des Mines de Nantes, Université de Nantes, CNRS-IN2P3, Nantes, France
[dd]Suranaree University of Technology, Nakhon Ratchasima, Thailand
[de]Technical University of Split FESB, Split, Croatia
[df]The Henryk Niewodniczanski Institute of Nuclear Physics, Polish Academy of Sciences, Cracow, Poland
[dg]The University of Texas at Austin, Physics Department, Austin, TX, United States
[dh]Universidad Autónoma de Sinaloa, Culiacán, Mexico

[di] Universidade de São Paulo (USP), São Paulo, Brazil
[dj] Universidade Estadual de Campinas (UNICAMP), Campinas, Brazil
[dk] Université de Lyon, Université Lyon 1, CNRS/IN2P3, IPN-Lyon, Villeurbanne, France
[dl] University of Houston, Houston, Texas, United States
[dm] University of Technology and Austrian Academy of Sciences, Vienna, Austria
[dn] University of Tennessee, Knoxville, Tennessee, United States
[do] University of Tokyo, Tokyo, Japan
[dp] University of Tsukuba, Tsukuba, Japan
[dq] Eberhard Karls Universität Tübingen, Tübingen, Germany
[dr] Variable Energy Cyclotron Centre, Kolkata, India
[ds] V. Fock Institute for Physics, St. Petersburg State University, St. Petersburg, Russia
[dt] Warsaw University of Technology, Warsaw, Poland
[du] Wayne State University, Detroit, Michigan, United States
[dv] Wigner Research Centre for Physics, Hungarian Academy of Sciences, Budapest, Hungary
[dw] Yale University, New Haven, Connecticut, United States
[dx] Yildiz Technical University, Istanbul, Turkey
[dy] Yonsei University, Seoul, South Korea
[dz] Zentrum für Technologietransfer und Telekommunikation (ZTT), Fachhochschule Worms, Worms, Germany

Abstract

In high–energy heavy–ion collisions, the correlations between the emitted particles can be used as a probe to gain insight into the charge creation mechanisms. In this article, we report the first results of such studies using the electric charge balance function in the relative pseudorapidity ($\Delta\eta$) and azimuthal angle ($\Delta\varphi$) in Pb–Pb collisions at $\sqrt{s_{NN}} = 2.76$ TeV with the ALICE detector at the Large Hadron Collider. The width of the balance function decreases with growing centrality (i.e. for more central collisions) in both projections. This centrality dependence is not reproduced by HIJING, while AMPT, a model which incorporates strings and parton rescattering, exhibits qualitative agreement with the measured correlations in $\Delta\varphi$ but fails to describe the correlations in $\Delta\eta$. A thermal blast wave model incorporating local charge conservation and tuned to describe the p_{T} spectra and v_2 measurements reported by ALICE, is used to fit the centrality dependence of the width of the balance function and to extract the average separation of balancing charges at freeze–out. The comparison of our results with measurements at lower energies reveals an ordering with $\sqrt{s_{NN}}$: the balance

functions become narrower with increasing energy for all centralities. This is consistent with the effect of larger radial flow at the LHC energies but also with the late stage creation scenario of balancing charges. However, the relative decrease of the balance function widths in $\Delta\eta$ and $\Delta\varphi$ with centrality from the highest SPS to the LHC energy exhibits only small differences. This observation cannot be interpreted solely within the framework where the majority of the charge is produced at a later stage in the evolution of the heavy–ion collision.

Keywords: Balance function, charge correlations, ALICE LHC

1. Introduction

According to Quantum ChromoDynamics (QCD), the theory that describes the strong interaction, at sufficiently high energy densities and temperatures, a new phase of matter exists in which the constituents, the quarks and the gluons, are deconfined [1]. This new state of matter is called the Quark Gluon Plasma (QGP). Its creation in the laboratory, the corresponding verification of its existence and the subsequent study of its properties are the main goals of the ultrarelativistic heavy–ion collision programs. Convincing experimental evidences for the existence of a deconfined phase have been published already at RHIC energies [2]. Recently, the first experimental results from the heavy–ion program of the LHC experiments provided additional indication [3, 4] for the existence of this state of matter at this new energy regime.

Among the different observables, such as the anisotropic flow [3] or the energy loss of high transverse momentum particles [4], the charge balance functions are suggested to be sensitive probes of the properties of the system, providing valuable insight into the charge creation mechanism and can be used to address fundamental questions concerning hadronization in heavy–ion collisions [5].

The system that is produced in a heavy–ion collision undergoes an expansion, during which it exhibits collective behavior and can be described in terms of hydrodynamics [6]. A pair of particles of opposite charge that is created during this stage is subject to the collective motion of the system, which transforms the correlations in coordinate space into correlations in momentum space. The subsequent rescattering phase after the hadronization will also affect the final measured degree of correlation. The balance function

being a sensitive probe of the balancing charge distribution in momentum space, quantifies these effects. The final degree of correlation is reflected in the balance function distribution and consequently in its width. It was suggested in [5] that narrow distributions correspond to a system that consists of particles that are created close to the end of the evolution. It was also suggested that a larger width may signal the creation of balancing charges at the first stages of the system's evolution [5].

The balance function describes the conditional probability that a particle in a bin P_1 in momentum space will be accompanied (balanced) by a particle of opposite charge with momentum P_2. The general definition is given in Eq. 1:

$$B_{ab}(P_2|P_1) = \frac{1}{2}\Big(C_{ab}(P_2|P_1) + C_{ba}(P_2|P_1)$$

$$- C_{bb}(P_2|P_1) - C_{aa}(P_2|P_1)\Big), \qquad (1)$$

where $C_{ab}(P_2|P_1) = N_{ab}(P_2|P_1)/N_b(P_1)$ is the distribution of pairs of particles, of type a and b, with momenta P_2 and P_1, respectively, normalized to the number of particles b. Particles a and b could come from different particle species (e.g. π^+–π^-, K^+–K^-, p–$\overline{\mathrm{p}}$). In this article, a refers to all positive and b to all negative particles. This analysis is performed for both particles in the pseudorapiity intervals $|\eta| < 0.8$. We assume that the balance function is invariant over pseudorapidity in this region, and report the results in terms of the relative pseudorapidity $\Delta\eta = \eta_b - \eta_a$ and the relative azimuthal angle $\Delta\varphi = \varphi_b - \varphi_a$, by averaging the balance function over the position of one of the particles (similar equation is used for $B(\Delta\varphi)$):

$$B_{+-}(\Delta\eta) = \frac{1}{2}\Big(C_{+-}(\Delta\eta) + C_{-+}(\Delta\eta) - C_{--}(\Delta\eta) - C_{++}(\Delta\eta)\Big). \qquad (2)$$

Each term of Eq. 2, is corrected for detector and tracking inefficiencies as well as for acceptance effects, similar to what is proposed in [7], and can be written as $C_{ab} = (N_{ab}/N_b)/f_{ab}$. The factors f_{ab} (where in the case of charged particles, a and b correspond to the charge i.e. f_{+-}, f_{-+}, f_{++} and f_{--}) represent the probability that given a particle a is reconstructed, a second

particle emitted at a relative pseudorapidity or azimuthal angle ($\Delta\eta$ or $\Delta\varphi$, respectively), would also be detected. These terms are defined as the product of the single particle tracking efficiency $\varepsilon(\eta, \varphi, p_{\mathrm{T}})$ and the acceptance term $\alpha(\Delta\eta, \Delta\varphi)$. The way they are extracted in this analysis is described in one of the following sections.

For a neutral system, every charge has an opposite balancing partner and the balance function would integrate to unity. However, this normalization does not hold if not all charged particles are included in the calculation due to specific momentum range or particle type selection.

The width of the balance function distribution can be used to quantify how tightly the balancing charges are correlated. It can be characterized by the average $\langle\Delta\eta\rangle$ or $\langle\Delta\varphi\rangle$ in case of studies in pseudorapidity or the azimuthal angle, respectively. The mathematical expression for the case of correlations in pseudorapidity is given in Eq. 3 (similar for $\langle\Delta\varphi\rangle$).

$$\langle\Delta\eta\rangle = \sum_{i=1}^{k} [B_{+-}(\Delta\eta_i) \cdot \Delta\eta_i] / \sum_{i=1}^{k} B_{+-}(\Delta\eta_i), \tag{3}$$

where $B_{+-}(\Delta\eta_i)$ is the balance function value for each bin $\Delta\eta_i$, with the sum running over all bins k.

Experimentally, the balance function for non–identified particles was studied by the STAR collaboration in Au–Au collisions at $\sqrt{s_{NN}} = 130$ GeV [8], followed by the NA49 experiment in Pb–Pb collisions at the highest SPS energy [9]. Both experiments reported the narrowing of the balance function in $\Delta\eta$ in more central compared to peripheral collisions. The results were qualitatively in agreement with theoretical expectations for a system with a long-lived QGP phase and exhibiting delayed hadronization. These results triggered an intense theoretical investigation of their interpretation [10, 11, 12, 13, 14, 15, 16]. In [10], it was suggested that the balance function could be distorted by the excess of positive charges due to the protons of the incoming beams (unbalanced charges). This effect is expected to be reduced at higher collision energy, leaving a system at mid–rapidity that is net–baryon free. Also in [10], it was proposed to perform balance function studies in terms of the relative invariant momentum of the particle pair, to eliminate the sensitivity to collective flow. In [11], it was shown that purely hadronic models predict a modest broadening of the balance function for

central heavy–ion collisions, contrary to the experimentally measured narrowing. It was also shown that thermal models were in agreement with the (at that time) published data, concluding that charge conservation is local at freeze–out, consistent with the delayed charged-creation scenario [11]. Similar agreement with the STAR data was reported in [12], where a thermal model that included resonances was used. In [13], the author showed that the balance function, when measured in terms of the relative azimuthal angle of the pair, is a sensitive probe of the system's collective motion and in particular of its radial flow. In [14], it was suggested that radial flow is also the driving force of the narrowing of the balance function in pseudorapidity, with its width being inversely proportional to the transverse mass, $m_{\mathrm{T}} = \sqrt{m^2 + p_{\mathrm{T}}^2}$. In parallel in [15, 16], the authors attributed the narrowing of the balance function for more central collisions to short range correlations in the QGP at freeze–out.

Recently, the STAR collaboration extended their balance function studies in Au–Au collisions at $\sqrt{s_{NN}} = 200$ GeV [17], confirming the strong centrality dependence of the width in $\Delta\eta$ but also revealing a similar dependence in $\Delta\varphi$, the latter being mainly attributed to radial flow. Finally, in [18] the authors fitted the experimentally measured balance function at the top RHIC energies with a blast–wave parameterization and argued that in $\Delta\varphi$ the results could be explained by larger radial flow in more central collisions. However the results in $\Delta\eta$ could only be reproduced when considering the separation of charges at freeze–out implemented in the model. They also stressed the importance of performing a multi–dimensional analysis. In particular, they presented how the balance function measured with respect to the orientation of the reaction plane (i.e. the plane of symmetry of a collision defined by the impact parameter vector and the beam direction) could probe potentially one of the largest sources of background in studies related to parity violating effects in heavy–ion collisions [19].

In this article we report the first results of the balance function measurements in Pb–Pb collisions at $\sqrt{s_{NN}} = 2.76$ TeV with the ALICE detector [20, 21]. The article is organized as follows: Section 2 briefly describes the experimental setup, while details about the data analysis are presented in Section 3. In Section 4 we discuss the main results followed by a detailed comparison with different models in Section 5. In the same section we present the energy dependence of the balance function. We conclude with the summary and a short outlook.

2. Experimental setup

ALICE [21] is the dedicated heavy–ion detector at the LHC, designed to cope with the high charged–particle densities measured in central Pb–Pb collisions [22]. The experiment consists of a large number of detector subsystems inside a solenoidal magnet (0.5 T). The central tracking systems of ALICE provide full azimuthal coverage within a pseudorapidity window $|\eta| < 0.9$. They are also optimized to provide good momentum resolution ($\approx 1\%$ at $p_{\mathrm{T}} < 1$ GeV/c) and particle identification (PID) over a broad momentum range, the latter being important for the future, particle type dependent balance function studies.

For this analysis, the charged particles were reconstructed using the *Time Projection Chamber* (TPC) [23], which is the main tracking detector of the central barrel. In addition, a complementary analysis relying on the combined tracking of the TPC and the *Inner Tracking System* (ITS) was performed. The ITS consists of six layers of silicon detectors employing three different technologies. The two innermost layers are *Silicon Pixel Detectors* (SPD), followed by two layers of *Silicon Drift Detectors* (SDD). Finally the two outermost layers are double–sided *Silicon Strip Detectors* (SSD).

The position of the primary interaction was determined by the TPC and by the SPD, depending on the tracking mode used. A set of forward detectors, namely the VZERO scintillator arrays, were used in the trigger logic and also for the centrality determination [22]. The VZERO detector consists of two arrays of scintillator counters, the VZERO–A and the VZERO–C, positioned on each side of the interaction point. They cover the pseudorapidity ranges of $2.8 < \eta < 5.1$ and $-3.7 < \eta < -1.7$ for VZERO–A and VZERO–C, respectively.

For more details on the ALICE experimental setup, see [21].

3. Data analysis

Approximately 15×10^6 Pb–Pb events, recorded during the first LHC heavy–ion run in 2010 at $\sqrt{s_{NN}} = 2.76$ TeV, were analyzed. A minimum bias trigger was used, requiring two pixel chips hit in the SPD in coincidence with a signal in the VZERO–A and VZERO–C detectors. Measurements were also made with the requirement changed to a coincidence between signals from the two sides of the VZERO detectors. An offline event selection was also applied in order to reduce the contamination from background events, such as

electromagnetic and beam–gas interactions. All events were required to have a reconstructed vertex position along the beam axis (V_z) with $|V_z| < 10$ cm from the nominal interaction point.

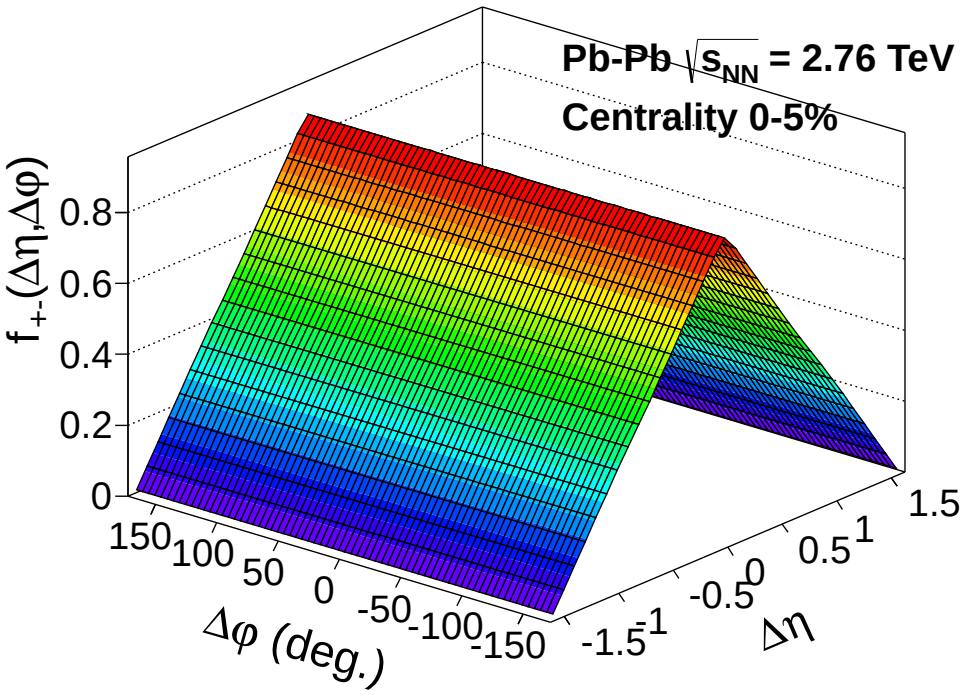

Figure 1: (color online). The correction factor $f_{+-}(\Delta\eta, \Delta\varphi)$ for the 5% most central Pb–Pb collisions, extracted from the single particle tracking efficiencies $\varepsilon(\eta, \varphi, p_{\mathrm{T}})$ and the acceptance terms $\alpha(\Delta\eta, \Delta\varphi)$ (see text for details).

The data were sorted according to centrality classes, reflecting the geometry of the collision (i.e. impact parameter), which span $0 - 80\%$ of the inelastic cross section. The $0 - 5\%$ bin corresponds to the most central (i.e. small impact parameter) and the $70 - 80\%$ class to the most peripheral (i.e. large impact parameter) collisions. The centrality of the collision was estimated using the charged particle multiplicity distribution and the distribution of signals from the VZERO scintillator detectors. Fitting these distributions with a Glauber model [24], the centrality classes are mapped to

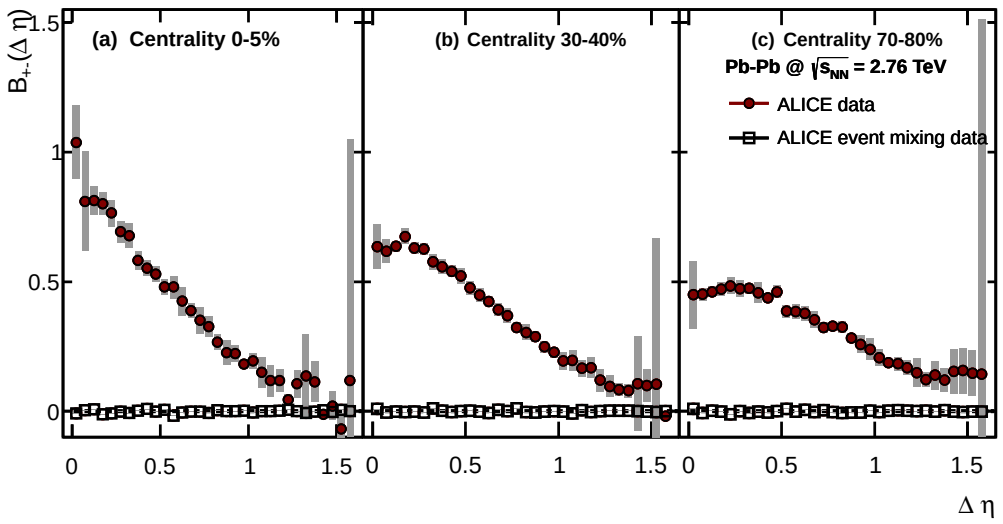

Figure 2: (color online). Balance function as a function of $\Delta\eta$ for different centrality classes: 0–5% (a), 30–40% (b) and 70–80%. Mixed events results, not corrected for the detector effects, are shown by open squares. See text for details.

the corresponding mean number of participating nucleons $\langle N_{\rm part}\rangle$ [25]. Different centrality estimators (i.e. TPC tracks, SPD clusters) were used to investigate the systematic uncertainties.

To select charged particles with high efficiency and to minimize the contribution from background tracks (i.e. secondary particles originating either from weak decays or from the interaction of particles with the material), all selected tracks were required to have at least 70 reconstructed space points out of the maximum of 159 possible in the TPC. The $\langle\chi^2\rangle$ per degree of freedom the momentum fit was required to be below 2. To further reduce the contamination from background tracks, a cut on the distance of closest approach between the tracks and the primary vertex (dca) was applied $(dca_{xy}/d_{xy})^2 + (dca_z/d_z)^2 < 1$ with $d_{xy} = 2.4$ cm and $d_z = 3.2$ cm. In the parallel analysis, with the combined tracking of the TPC and the ITS, the values of $d_{xy} = 0.3$ cm and $d_z = 0.3$ cm were used, profiting from the better dca resolution that the ITS provides. Finally, we report the results for the region of $|\eta| < 0.8$ and $0.3 < p_{\rm T} < 1.5$ GeV/c. The $p_{\rm T}$ range is chosen to ensure a high tracking efficiency (lower cut) and a minimum contribution from (mini–)jet correlations (upper cut).

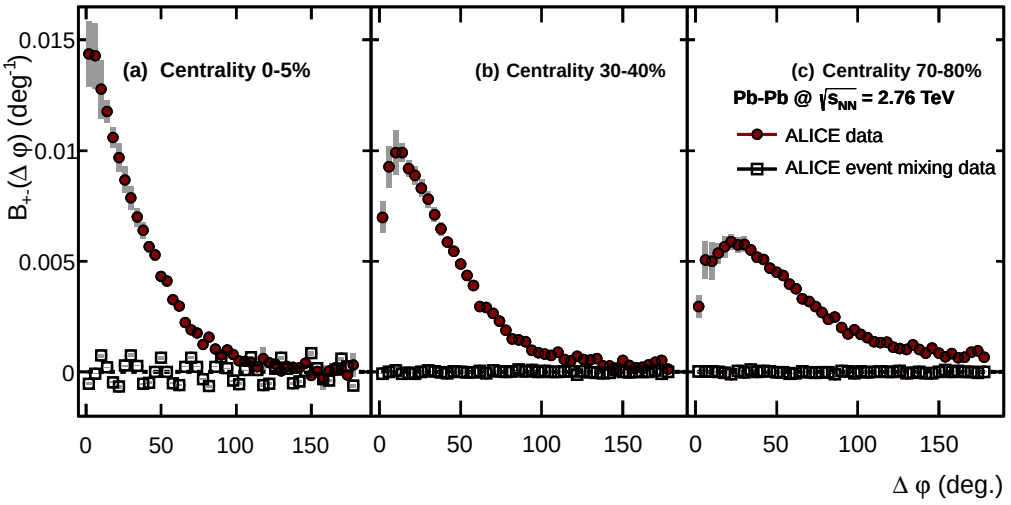

Figure 3: (color online). Balance function as a function of $\Delta\varphi$ for different centrality classes: 0–5% (a), 30–40% (b) and 70–80%. Mixed events results, not corrected for the detector effects, are shown by open squares. See text for details.

4. Results

As discussed in the introduction, the correction factors f_{+-}, f_{-+}, f_{++}, and f_{--} are needed to eliminate the dependence of the balance function on the detector acceptance and tracking inefficiencies. The tracking inefficiencies are extracted from a detailed Monte Carlo simulation of the ALICE detector based on GEANT3 [26]. The acceptance part of the correction factors, $\alpha(\Delta\eta, \Delta\varphi)$, is extracted from mixed events. The mixed events are generated by taking all two–particle non–same–event combinations for a collection of a few (≈ 5) events with similar values of the z position of the reconstructed vertex ($|\Delta V_z| < 5$ cm). In addition, the events used for the event mixing belonged to the same centrality class and had multiplicities that did not differ by more than 1–2%, depending on the centrality. Figure 1 presents the correction factor for the distribution of pairs of particles with opposite charge as a function of the relative pseudorapidity and azimuthal angle differences for the 5% most central Pb–Pb collisions. The maximum value is observed for $\Delta\eta = 0$ and is equal to the p_{T}–integrated single particle efficiency. The distribution decreases to ≈ 0 near the edge of the acceptance i.e. $|\Delta\eta| \approx 1.6$. This

reduction reflects the decrease of the probability of detecting both balancing charges as the relative pseudorapidity difference increases. The correction factor is constant as a function of $\Delta\varphi$.

The measured balance function is averaged over positive and negative values of $\Delta\eta$ ($\Delta\varphi$) and reported only for positive values. The integrals of the balance function over the reported region are close to 0.5, reflecting the fact that most of the balancing charges are distributed in the measured region.

Figure 2 presents the balance functions as a function of the relative pseudorapidity $\Delta\eta$ for three different centrality classes: the 0–5% (most central), the 30–40% (mid–central) and the 70–80% (most peripheral) centrality bins. It is seen that the balance function, in full circles, gets narrower for more central collisions. Figure 2 presents also the balance functions for mixed events, not corrected for detector effects, represented by the open squares. These balance functions, fluctuate around zero as expected for a totally uncorrelated sample where the charge is not conserved.

Figure 3 presents the balance functions as a function of the relative azimuthal angle for the same centrality classes as in Fig. 2. The balance functions calculated using mixed events and not corrected for the tracking efficiency exhibit a distinct modulation originating from the 18 sectors of the TPC. This modulation is more pronounced for more central collisions, since the charge dependent acceptance differences scale with multiplicity. The efficiency-corrected balance functions, represented by the full markers, indicate that these detector effects are successfully removed. Narrowing of the balance function in more central events has been also observed in this representation. A decrease of the balance function at small $\Delta\varphi$ (i.e. for $\Delta\varphi \leq 10^{\circ}$) can be observed for the mid–central and peripheral collisions. This can be attributed to short–range correlations between pairs of same and opposite charge, such as HBT and Coulomb effects [18].

In both Fig. 2 and Fig. 3 as well as in the next figures, the error bar of each point corresponds to the statistical uncertainty (typically the size of the marker). The systematic uncertainty is represented by the shaded band around each point. The origin and the value of the assigned systematic uncertainty on the width of the balance function, calculated for each centrality and for both $\Delta\eta$ and $\Delta\varphi$, will be discussed in the next paragraph.

The data sample was analyzed separately for two magnetic field configurations. The two data samples had comparable statistics. The maximum value of the systematic uncertainty, defined as half of the difference between the balance functions in these two cases, is found to be less than 1.3% over

all centralities. In addition, we estimated the contribution to the systematic uncertainty originating from the centrality selection, by determining the centrality not only with the VZERO detector but alternatively using the multiplicity of the TPC tracks or the number of clusters of the second SPD layer. This resulted in an additional maximum contribution to the estimated systematic uncertainty of 0.8% over all centralities. Furthermore, we investigated the influence of the ranges of the cuts in parameters such as the position of the primary vertex in the z coordinate, the dca, and the number of required TPC clusters. This was done by varying the relevant ranges, one at a time, and again assigning half of the difference between the lower and higher value of the width to the systematic uncertainty. The maximum contribution from these sources was estimated to be 1.3%, 1.1% and 1.3% for the three parameters, respectively. We also studied the influence of the different tracking modes used by repeating the analysis using tracks reconstructed by the combination of the TPC and the ITS (global tracking). The resulting maximum contribution to the systematic uncertainty of the width from this source is 1.1%, again over all centralities. Finally, the applied acceptance corrections result in large fluctuations of the balance function points for some centralities towards the edge of the acceptance (i.e. large values of $\Delta\eta$), which originates from the division of two small numbers. To account for this, we average over several bins at these high values of $\Delta\eta$ to extract the weighted average. This procedure results in an uncertainty that has a maximum value of 5% over all centralities. All these contributions are summarized in Table 1. The final systematic uncertainty for each centrality bin was calculated by adding all the different sources in quadrature. The resulting values for the 0–5%, 30–40% and 70–80% centrality bins were estimated to be 2.5%, 3.0% and 3.6%, respectively, in $\langle\Delta\eta\rangle$ (1.9%, 1.2% and 2.4%, respectively, in $\langle\Delta\varphi\rangle$).

5. Discussion

5.1. Centrality dependence

The width of the balance function (Eq. 3) as a function of the centrality percentile is presented in Fig. 4. Central (peripheral) collisions correspond to small (large) centrality percentile. The width is calculated in the entire interval where the balance function was measured (i.e. $0.0 < \Delta\eta < 1.6$ and $0^o < \Delta\varphi < 180^o$). Both results in terms of correlations in the relative pseudorapidity ($\langle\Delta\eta\rangle$–upper panel, Fig. 4–a) and the relative azimuthal angle

Table 1: The maximum value of the systematic uncertainties on the width of the balance function over all centralities for each of the sources studied.

Systematic Uncertainty		
Category	Source	Value (max)
Magnetic field	(++)/(- -)	1.3%
Centrality estimator	VZERO, TPC, SPD	0.8%
Cut variation	dca	1.3%
	$N_{clusters}(TPC)$	1.1%
	ΔV_z	1.3%
Tracking	TPC, Global	1.1%
Binning	Extrapolation to large $\Delta\eta$	5.0%

($\langle\Delta\varphi\rangle$–lower panel, Fig. 4–b) are shown. The experimental data points, represented by the full red circles, exhibit a strong centrality dependence: more central collisions correspond to narrower distributions (i.e. moving from right to left along the x–axis) for both $\Delta\eta$ and $\Delta\varphi$. Our results are compared to different model predictions, such as HIJING [27] and different versions of a multi–phase transport model (AMPT) [28]. The error bars in the results from these models represent the statistical uncertainties.

The points from the analysis of HIJING Pb–Pb events at $\sqrt{s_{NN}} = 2.76$ TeV, represented by the blue triangles, show little centrality dependence in both projections. The slightly narrower balance functions for central collisions might be related to the fact that HIJING is not just a simple superposition of single pp collisions; jet–like effects as well as increased resonance yields in central collisions could be reflected as additional correlations. The balance function widths generated by HIJING are much larger than those measured in the data, consistent with the fact that the model lacks collective flow.

In addition, we compare our data points to the results from the analysis of events from three different versions of AMPT in Fig. 4. The AMPT model consists of two different configurations: the *default* and the *string melting*. Both are based on HIJING to describe the initial conditions. The partonic evolution is described by the Zhang's parton cascade (ZPC) [29]. In the *default* AMPT model, partons are recombined with their parent strings when they stop interacting, and the resulting strings are converted to hadrons using the Lund string fragmentation model. In the *string melting* configuration a quark coalescence model is used instead to combine partons into hadrons. The final part of the whole process, common between the two configura-

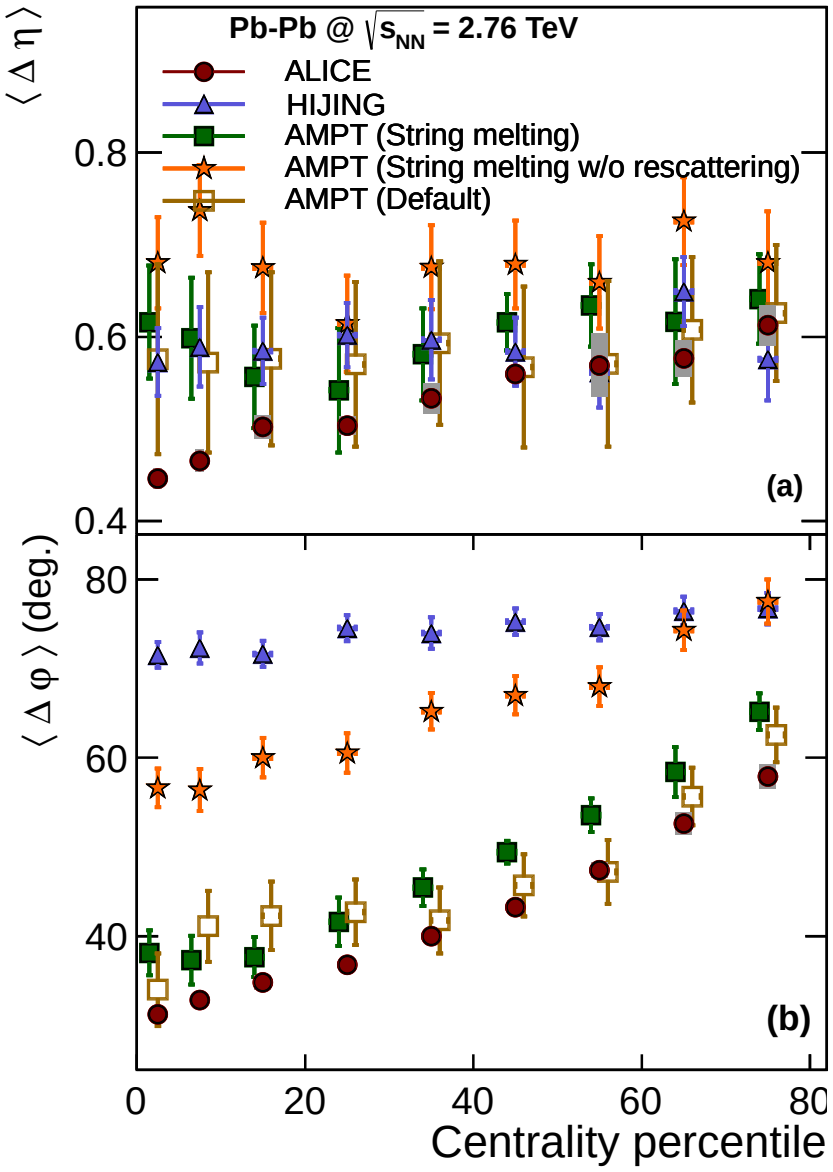

Figure 4: (color online). The centrality dependence of the width of the balance function $\langle\Delta\eta\rangle$ and $\langle\Delta\varphi\rangle$, for the correlations studied in terms of the relative pseudorapidity and the relative azimuthal angle, respectively. The data points are compared to the predictions from HIJING [27], and AMPT [28].

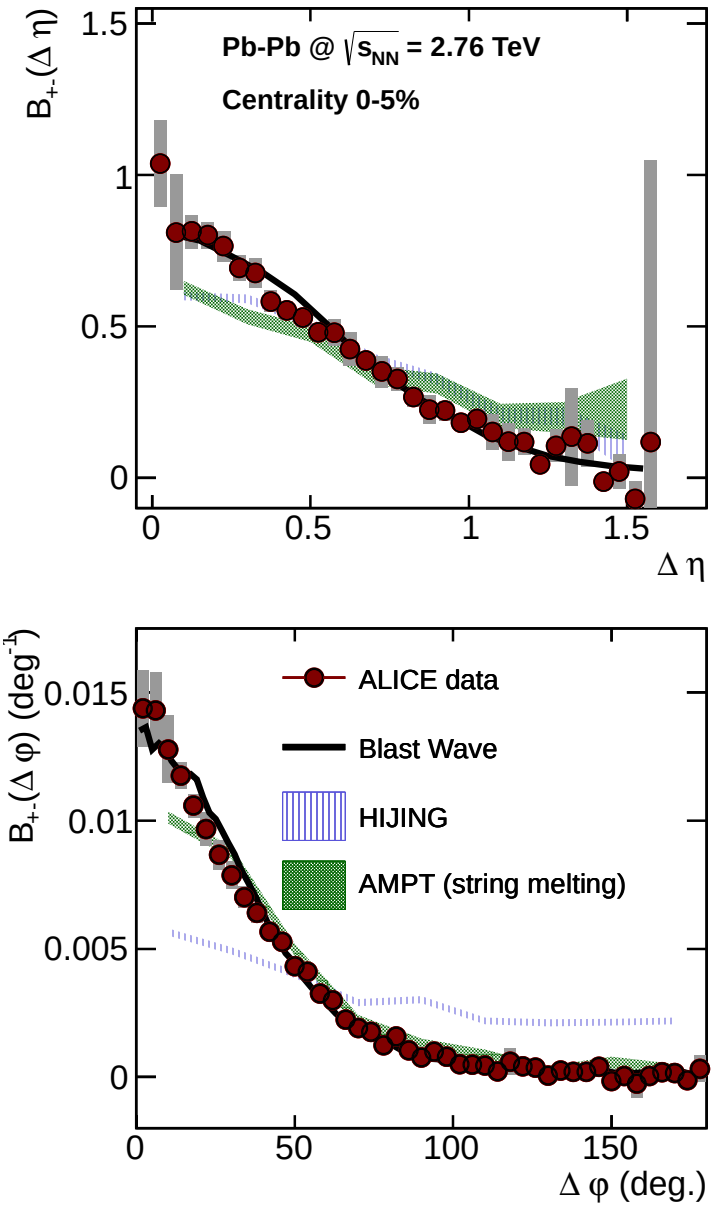

Figure 5: (color online). The balance functions for the 5% most central Pb–Pb collisions measured by ALICE as a function of the relative pseudorapidity (a) and the relative azimuthal angle (b). The experimental points are compared to predictions from HIJING [27], AMPT [28] and from a thermal blast wave [31, 32].

tions, consists of the hadronic rescattering which also includes the decay of resonances.

The filled green squares represent the results of the analysis of the *string melting* AMPT events with parameters tuned [30] to reproduce the measured elliptic flow (v_2) values of non–identified particles at the LHC [3]. The width of the balance functions when studied in terms of the relative pseudorapidity exhibit little centrality dependence despite the fact that the produced system exhibits significant collective behavior [30]. However, the width of the balance function in $\Delta\varphi$ is in qualitative agreement with the centrality dependence of the experimental points. This is consistent with the expectation that the balance function when studied as a function of $\Delta\varphi$ can be used as a measure of radial flow of the system, as suggested in [13, 18]. We also studied the same AMPT configuration, i.e. the *string melting*, this time switching off the last part where the hadronic rescattering takes place, without altering the decay of resonances. The resulting points, indicated with the orange filled stars in Fig. 4, demonstrate a similar qualitative behavior as in the previous case: no centrality dependence of $\langle\Delta\eta\rangle$ and a significant decrease of $\langle\Delta\varphi\rangle$ for central collisions. On a quantitative level though, the widths in both projections are larger than the ones obtained in the case where hadronic rescattering is included. This can be explained by the fact that within this model, a significant part of radial flow of the system is built during this very last stage of the system's evolution. Therefore, the results are consistent with the picture of having the balancing charges more focused under the influence of this collective motion, which is reflected in a narrower balance function distribution. In addition, we analyzed AMPT events produced using the *default* configuration, which results in smaller v_n flow coefficients but harder spectra than the *string melting*. The extracted widths of the balance functions are represented by the open brown squares and exhibit similar behavior as the results from the *string melting* configuration. In particular, the width in $\Delta\eta$ shows little centrality dependence while the values are in agreement with the ones calculated from the *string melting*. The width in $\Delta\varphi$ shows similar (within the statistical uncertainties) quantitative centrality dependence as the experimental data points. However, these latter results exhibit a systematically lower value of the width for this version of AMPT compared to the *string melting* configuration. This latter effect is consistent with the observation of having a system exhibiting larger radial flow with

the *default* version.[3]

Finally, we fit the experimentally measured values with a thermal blast–wave model [31, 32]. This model, assumes that the radial expansion velocity is proportional to the distance from the center of the system and takes into account the resonance production and decay. It also incorporates the local charge conservation, by generating ensembles of particles with zero total charge. Each particle of an ensemble is emitted by a fluid element with a common collective velocity following the single–particle blast–wave parameterization with the additional constraint of being emitted with a separation at kinetic freeze–out from the neighboring particle sampled from a Gaussian with a width denoted as σ_η and σ_φ in the pseudorapidity space and the azimuthal angle, respectively. The procedure that we followed started from tuning the input parameters of the model to match the average $p_{\rm T}$ values extracted from the analysis of identified particle spectra [34] as well as the v_2 values for non–identified particles reported by ALICE [3]. We then adjust the widths of the parameters σ_η and σ_φ to match the experimentally measured widths of the balance function, $\langle\Delta\eta\rangle$ and $\langle\Delta\varphi\rangle$. The resulting values of σ_η and σ_φ are listed in Table 2. We find that σ_η starts from 0.28 ± 0.05 for the most central Pb–Pb collisions reaching 0.52 ± 0.07 for the most peripheral, while σ_φ starts from 0.30 ± 0.10 evolving to 0.76 ± 0.01 for the 60–70% centrality bin.

Figure 5 presents the detailed comparison of the model results with the measured balance functions as a function of $\Delta\eta$ (a) and $\Delta\varphi$ (b) for the 5% most central Pb–Pb collisions. The data points are represented by the full markers and are compared with HIJING (dotted blue line), AMPT *string melting* (dashed green line) and the thermal blast–wave (full black line). The distributions for HIJING and AMPT are normalized to the same integral to facilitate the direct comparison of the shapes and the widths. It is seen that for correlations in the relative pseudorapidity, both HIJING and AMPT result in similarly wider distributions. As mentioned before, the blast–wave model is tuned to reproduce the experimental points, so it is not surprising that the relevant curve not only reproduces the same narrow distribution but describes fairly well also its shape. For the correlations in $\Delta\varphi$ the HIJING

[3]We recently confirmed that AMPT does not conserve the charge. The influence of this effect to our measurement can not be easily quantified. However we still consider interesting and worthwhile to point out that this model describes in a qualitative (and to some extent quantitative) way the centrality dependence of $\langle\Delta\varphi\rangle$.

Table 2: The values of σ_η and σ_φ extracted by fitting the centrality dependence of both $\langle\Delta\eta\rangle$ and $\langle\Delta\varphi\rangle$ with the blast–wave parameterization of [31, 32].

Results from the fit with the blast–wave model		
Centrality	σ_η	σ_φ
0–5%	0.28 ± 0.05	0.30 ± 0.10
5–10%	0.32 ± 0.05	0.35 ± 0.07
10–20%	0.31 ± 0.05	0.36 ± 0.08
20–30%	0.36 ± 0.03	0.43 ± 0.05
30–40%	0.43 ± 0.04	0.52 ± 0.05
40–50%	0.42 ± 0.04	0.54 ± 0.06
50–60%	0.44 ± 0.07	0.64 ± 0.06
60–70%	0.52 ± 0.07	0.76 ± 0.01

curve clearly results in a wider balance function distribution. On the other hand, there is a very good agreement between the AMPT curve and the measured points, with the exception of the first bins (i.e. small relative azimuthal angles) where the magnitude of $B_{+-}(\Delta\varphi)$ is significantly larger in real data. This suggests that there are additional correlations present in these small ranges of $\Delta\varphi$ in data than what the model predicts.

5.2. Energy dependence

Figure 6 presents the comparison of our results for the centrality dependence (i.e. as a function of the centrality percentile) of the width of the balance function, $\langle\Delta\eta\rangle$ (Fig. 6–a) and $\langle\Delta\varphi\rangle$ (Fig. 6–b), with results from STAR [17] in Au–Au collisions at $\sqrt{s_{NN}} = 200$ GeV (stars). The ALICE points have been corrected for acceptance and detector effects, using the correction factors f_{ab}, discussed in the introduction. To make a proper comparison with the STAR measurement, where such a correction was not applied, we employ the procedure suggested in [7] to the RHIC points. Based on the assumption of a boost–invariant system the balance function studied in a given pseudorapidity window $B_{+-}(\Delta\eta|\eta_{\rm max})$ can be related to the balance function for an infinite interval according to the formula of Eq. 4

$$B_{+-}(\Delta\eta|\eta_{\rm max}) = B_{+-}(\Delta\eta|\infty) \cdot \Big(1 - \frac{\Delta\eta}{\eta_{\rm max}}\Big). \quad (4)$$

This procedure results in similar corrections as to the case where the f_{ab} are used, if the acceptance is flat in η (which is a reasonable assumption for the acceptance of STAR).[4]

While the centrality dependence is similar for both measurements, the widths are seen to be significantly narrower at the LHC energies. This is consistent with the idea of having a system exhibiting larger radial flow at the LHC with respect to RHIC [3] while having a longer–lived QGP phase [33] with the consequence of a smaller separation between charge pairs when created at hadronization. However, it is seen that the relative decrease of the width between central and peripheral collisions seems to be similar between the two energies. This observation could challenge the interpretation of the narrowing of the width in $\Delta\eta$ as primarily due to the late stage creation of balancing charges.

To further quantify the previous observation, Fig. 7 presents the relative decrease of $\langle\Delta\eta\rangle$ (a) and $\langle\Delta\varphi\rangle$ (b) from peripheral to central collisions as a function of the mean number of participating nucleons, $\langle N_{\rm part}\rangle$, for the highest SPS[5] [9] and RHIC [17] energies, compared to the values reported in this article. In this figure, central (peripheral) collisions correspond to high (low) number of $\langle N_{\rm part}\rangle$. The choice of the representation as a function of $\langle N_{\rm part}\rangle$ is mainly driven by the apparent better scaling compared to the centrality percentile. It is seen that in terms of correlations in relative pseudorapidity the data points at the different energies are in fairly good agreement within the uncertainties, resulting though into an additional, marginal decrease for the 0–5% most central collisions of $\approx (9.5 \pm 2.0\,(stat) \pm 2.5\,(syst))\%$ compared to the RHIC point. On the other hand, $\langle\Delta\varphi\rangle/\langle\Delta\varphi\rangle_{peripheral}$ exhibits a decrease of $\approx (14.0 \pm 1.3\,(stat) \pm 1.9\,(syst))\%$ between the most central Au–Au collisions at $\sqrt{s_{NN}} = 200$ GeV and the results reported in this article. This could be attributed to the additional increase in radial flow between central and peripheral collisions at the LHC compared to RHIC energies. Another contribution might come from the bigger influence from jet–like structures at the LHC with respect to RHIC that results in particles being emitted prefer-

[4]We do not compare our results to the data from the NA49 experiment at SPS in this figure, for two reasons. Firstly, the balance function in that experiment was not measured at mid-rapidity. Secondly, the non-uniform acceptance in pseudorapidity makes the simplified correction of Eq. 4 invalid.

[5]We include the NA49 points in this representation since the ratio to the peripheral results should cancel out the acceptance effects to first order.

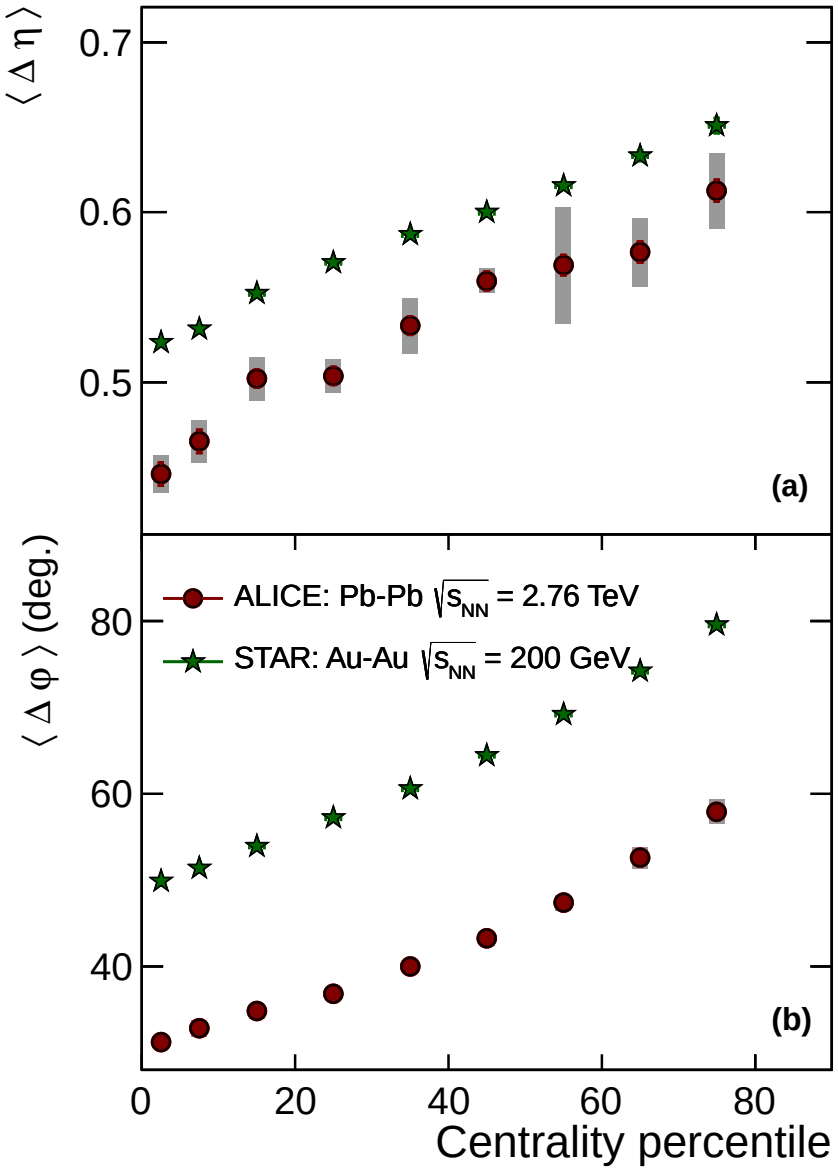

Figure 6: (color online). The centrality dependence of the balance function width $\langle\Delta\eta\rangle$ (a) and $\langle\Delta\varphi\rangle$ (b). The ALICE points are compared to results from STAR [17]. The STAR results have been corrected for the finite acceptance as suggested in [7].

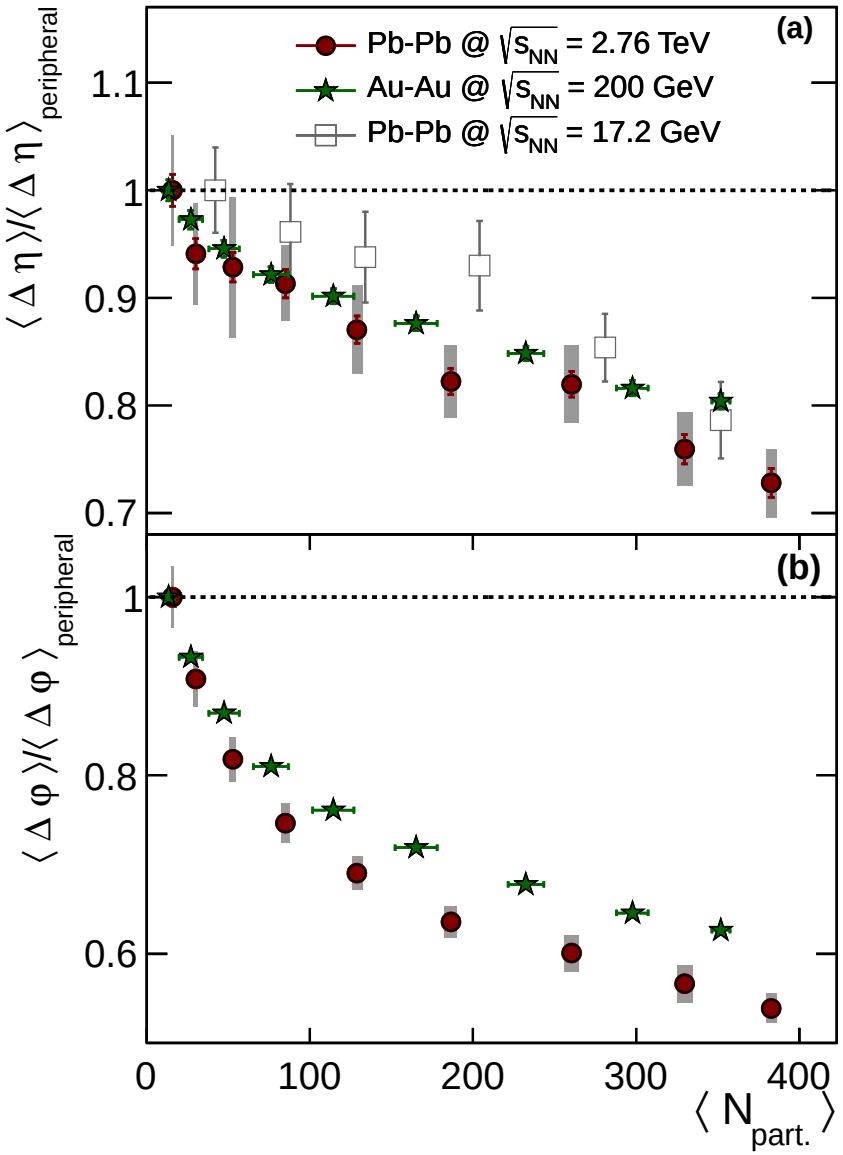

Figure 7: (color online). The centrality dependence of the relative decrease of the width of the balance function in the relative pseudorapidity (a) and relative azimuthal angle (b). The ALICE points are compared to results for the highest SPS [9] and RHIC [17] energies.

entially in cones with small opening angles. Contrary to $\langle\Delta\varphi\rangle/\langle\Delta\varphi\rangle_{peripheral}$, this strikingly marginal decrease of $\langle\Delta\eta\rangle/\langle\Delta\eta\rangle_{peripheral}$ between the three colliding energy regimes that differ more than an order of magnitude, can not be easily understood solely within the framework of the late stage creation of charges.

6. Summary

This article reported the first measurements of the balance function for charged particles in Pb–Pb collisions at the LHC using the ALICE detector. The balance function was studied both, in relative pseudorapidity ($\Delta\eta$) and azimuthal angle ($\Delta\varphi$). The widths of the balance functions, $\langle\Delta\eta\rangle$ and $\langle\Delta\varphi\rangle$, are found to decrease when moving from peripheral to central collisions. The results are consistent with the picture of a system exhibiting larger radial flow in central collisions but also whose charges are created at a later stage of the collision. While HIJING is not able to reproduce the observed centrality dependence of the width in either projection, AMPT tuned to describe the v_2 values reported by ALICE seems to agree qualitatively with the centrality dependence of $\langle\Delta\varphi\rangle$ but fails to reproduce the dependence of $\langle\Delta\eta\rangle$. A thermal blast–wave model incorporating the principle of local charge conservation was fitted to the centrality dependence of $\langle\Delta\eta\rangle$ and $\langle\Delta\varphi\rangle$. The resulting values of the charge separation at freeze–out can be used to constrain models describing the hadronization processes. The comparison of the results with those from lower energies showed that the centrality dependence of the width, in both the relative pseudorapidity and azimuthal angle, when scaled by the most peripheral widths, exhibits minor differences between RHIC and LHC.

These studies will soon be complemented by and extended to the correlations of identified particles in an attempt to probe the chemical evolution of the produced system, to quantify the influence of radial flow to the narrowing of the balance function width in more central collisions and to further constrain the parameters of the models used to describe heavy–ion collisions.

We would like to thank Scott Pratt for providing us with the blast wave model calculations and fruitful discussions. The ALICE collaboration would like to thank all its engineers and technicians for their invaluable contributions to the construction of the experiment and the CERN accelerator teams for the outstanding performance of the LHC complex.
The ALICE collaboration acknowledges the following funding agencies for

their support in building and running the ALICE detector:
State Committee of Science, Calouste Gulbenkian Foundation from Lisbon and Swiss Fonds Kidagan, Armenia;
Conselho Nacional de Desenvolvimento Científico e Tecnológico (CNPq), Financiadora de Estudos e Projetos (FINEP), Fundação de Amparo à Pesquisa do Estado de São Paulo (FAPESP);
National Natural Science Foundation of China (NSFC), the Chinese Ministry of Education (CMOE) and the Ministry of Science and Technology of China (MSTC);
Ministry of Education and Youth of the Czech Republic;
Danish Natural Science Research Council, the Carlsberg Foundation and the Danish National Research Foundation;
The European Research Council under the European Community's Seventh Framework Programme;
Helsinki Institute of Physics and the Academy of Finland;
French CNRS-IN2P3, the 'Region Pays de Loire', 'Region Alsace', 'Region Auvergne' and CEA, France;
German BMBF and the Helmholtz Association;
General Secretariat for Research and Technology, Ministry of Development, Greece;
Hungarian OTKA and National Office for Research and Technology (NKTH);
Department of Atomic Energy and Department of Science and Technology of the Government of India;
Istituto Nazionale di Fisica Nucleare (INFN) and Centro Fermi - Museo Storico della Fisica e Centro Studi e Ricerche "Enrico Fermi", Italy;
MEXT Grant-in-Aid for Specially Promoted Research, Japan;
Joint Institute for Nuclear Research, Dubna;
National Research Foundation of Korea (NRF);
CONACYT, DGAPA, México, ALFA-EC and the HELEN Program (High-Energy physics Latin-American–European Network);
Stichting voor Fundamenteel Onderzoek der Materie (FOM) and the Nederlandse Organisatie voor Wetenschappelijk Onderzoek (NWO), Netherlands;
Research Council of Norway (NFR);
Polish Ministry of Science and Higher Education;
National Authority for Scientific Research - NASR (Autoritatea Naţională pentru Cercetare Ştiinţifică - ANCS);
Ministry of Education and Science of Russian Federation, International Science and Technology Center, Russian Academy of Sciences, Russian Federal

Agency of Atomic Energy, Russian Federal Agency for Science and Innovations and CERN-INTAS;
Ministry of Education of Slovakia;
Department of Science and Technology, South Africa;
CIEMAT, EELA, Ministerio de Educación y Ciencia of Spain, Xunta de Galicia (Consellería de Educación), CEADEN, Cubaenergía, Cuba, and IAEA (International Atomic Energy Agency);
Swedish Research Council (VR) and Knut & Alice Wallenberg Foundation (KAW);
Ukraine Ministry of Education and Science;
United Kingdom Science and Technology Facilities Council (STFC);
The United States Department of Energy, the United States National Science Foundation, the State of Texas, and the State of Ohio.

References

[1] H. Satz, Rep. Prog. Phys. **63**, (2000) 1511;
S.A. Bass, M. Gyulassy, H. Stöcker, W. Greiner, J. Phys. **G25**, (1999) R1;
E.V. Shuryak, Phys. Rep. **115**, (1984) 151;
J. Cleymans, R.V. Gavai, E. Suhonen, Phys. Rep. **130**, (1986) 217.

[2] I. Arsene *et al.* [BRAHMS Collaboration], Nucl. Phys. **A757**, (2005) 1.
K. Adcox *et al.* [PHENIX Collaboration], Nucl. Phys. **A757**, (2005) 184.
B. B. Back *et al.* [PHOBOS Collaboration], Nucl. Phys. **A757**, (2005) 28.
J. Adams *et al.* [STAR Collaboration], Nucl. Phys. **A757**, (2005) 102.

[3] K. Aamodt *et al.* [ALICE Collaboration], Phys. Rev. Lett. **105**, (2010) 252302.
K. Aamodt *et al.* [ALICE Collaboration], Phys. Rev. Lett. **107**, (2011) 032301.

[4] G. Aad *et al.* [ATLAS Collaboration], Phys. Rev. Lett. **105**, (2010) 252303.
K. Aamodt *et al.* [ALICE Collaboration], Phys. Lett. **B696**, (2011) 30.

[5] S. A. Bass, P. Danielewicz and S. Pratt , Phys. Rev. Lett. **85**, (2000) 2689.

[6] P. Kolb and U. Heinz, arXiv:nucl-th/0305084

[7] S. Jeon and S. Pratt, Phys. Rev. **C65**, (2002) 044902.

[8] J. Adams *et al.* [STAR Collaboration], Phys. Rev. Lett. **90**, (2003) 172301.

[9] C. Alt *et al.* [NA49 Collaboration], Phys. Rev. **C71**, (2005) 034903.
C. Alt *et al.* [NA49 Collaboration], Phys. Rev. **C76**, (2007) 024914.

[10] S. Pratt and S. Cheng, Phys. Rev. **C68**, (2003) 014907.

[11] S. Cheng *et al.*, Phys. Rev. **C69**, (2004) 054906.

[12] W. Florkowski, P. Bozek and W. Broniowski, J. Phys. **G30**, (2004) S1321.
W. Florkowski, P. Bozek and W. Broniowski, Heavy Ion Phys. **A21**, (2004) 49.
W. Florkowski, P. Bozek and W. Broniowski, Acta Phys. Hung. **A22**, (2005) 149.

[13] P. Bozek, Phys. Lett. **B609**. (2005) 247.

[14] S. Voloshin, Phys. Lett. **B632**, (2006) 490.

[15] A. Bialas and J. Rafelski, Phys. Lett. **B633**, (2006) 488.

[16] A. Bialas, Phys. Lett. **B579**, (2004) 31.
A. Bialas, Phys. Rev. **C83**, (2011) 024914.

[17] M. M. Aggarwal *et al.* [STAR Collaboration], Phys. Rev. **C82**, (2010) 024905.

[18] S. Schlichting and S. Pratt, Phys.Rev. **C83**, (2011) 014913.

[19] B. Abelev *et al.* [ALICE Collaboration], arXiv:1207.0900 [nucl-ex].

[20] K. Aamodt *et al.* [ALICE Collaboration], J. Phys. **G30**, (2004) 1517;
K. Aamodt *et al.* [ALICE Collaboration], J. Phys. **G32**, (2006) 1295.

[21] K. Aamodt *et al.* [ALICE Collaboration], JINST **3**, (2008) S08002.

[22] K. Aamodt *et al.* [ALICE Collaboration], Phys. Rev. Lett. **105**, (2010) 252301.

[23] J. Alme *et al.* [ALICE Collaboration], arXiv:1001.1950 [physics.ins-det].

[24] B. Alver, M. Baker, C. Loizides, and P. Steinberg, (2008), arXiv:0805.4411 [nucl-ex].

[25] K. Aamodt *et al.* [ALICE Collaboration], Phys. Rev. Lett. **106**, (2011) 032301.

[26] R. Brun *et al.*, 1985 GEANT3 User Guide, CERN Data Handling Division DD/EE/841;
R. Brun *et al.*, 1994 CERN Program Library Long Write-up, W5013, GEANT Detector Description and Simulation Tool.

[27] M. Gyulassy and X. N. Wang, Comput. Phys. Commun. **83**, 307 (1994).
X. N. Wang and M. Gyulassy, Phys. Rev. **D44**, 3501 (1991).

[28] B. Zhang *et al.*, Phys. Rev. **C61**, (2000) 067901.
Z. W. Lin *et al.*, Phys.Rev. **C64** (2001) 011902.
Z. W. Lin *et al.*, Phys. Rev. **C72**, (2005) 064901.

[29] B. Zhang, Comput. Phys. Commun. **109**, (1998) 193.

[30] J. Xu and C. M. Ko, Phys. Rev. **C83** (2011) 034904.
J. Xu and C. M. Ko, Phys.Rev. **C84**, (2011) 044907.

[31] S. Pratt, Phys. Rev. **C85**, (2012) 014904.

[32] S. Pratt, Phys. Rev. Lett. **108**, (2012) 212301.

[33] K. Aamodt *et al.* [ALICE Collaboration], Phys. Lett. **B696**, (2011) 328.

[34] J. Schukraft (for the ALICE Collaboration), J. Phys. **G38**, (2011) 124003.

[35] B. Abelev *et al.* [ALICE Collaboration], arxiv:1207.6068 [nucl-ex] (submitted in Phys. Rev. Lett.).

[36] C. Pruneau, S. Gavin, S. Voloshin, Phys. Rev. **C66**, (2002) 044904;
J. Nystrand, E. Stenlund, H. Tydesjo, Phys. Rev. **C68**, (2003) 034902.

[37] B. I. Abelev *et al.* [STAR Collaboration], Phys. Rev. **C79**, (2009) 024906; J. Adams *et al.* [STAR Collaboration], Phys. Rev. **C68**, (2003) 044905.

[38] S. Jeon, V. Koch, Phys. Rev. Lett. **85**, (2000) 2076; S. Jeon, V. Koch, Phys. Rev. Lett. **83**, (1999) 5435.